AD-A179 423 GAS TURBINE COMBUSTOR AND ENGINE AUGMENTOR TUBE SOOTING 1/1
CHARACTERISTICS(U) NAVAL POSTGRADUATE SCHOOL MONTEREY
CA J S BENNETT ET AL. DEC 86 NPS67-86-004

UNCLASSIFIED F/G 21/2 NL

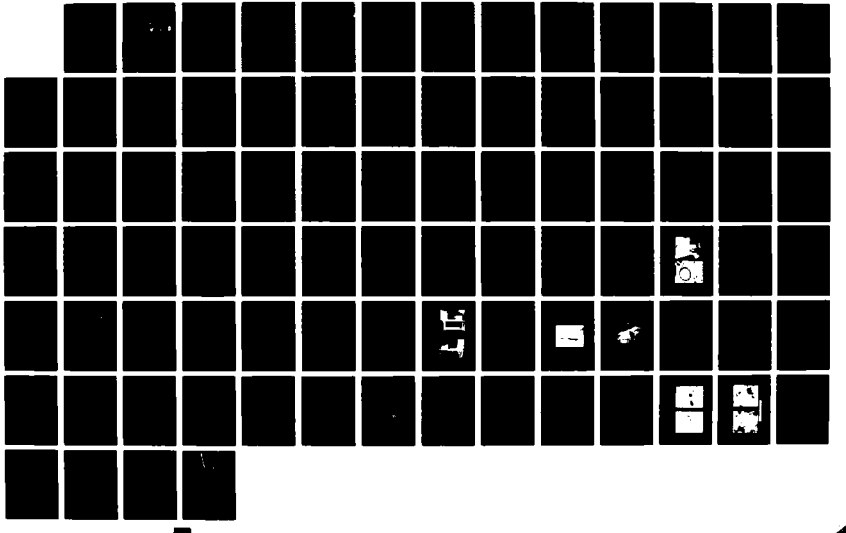

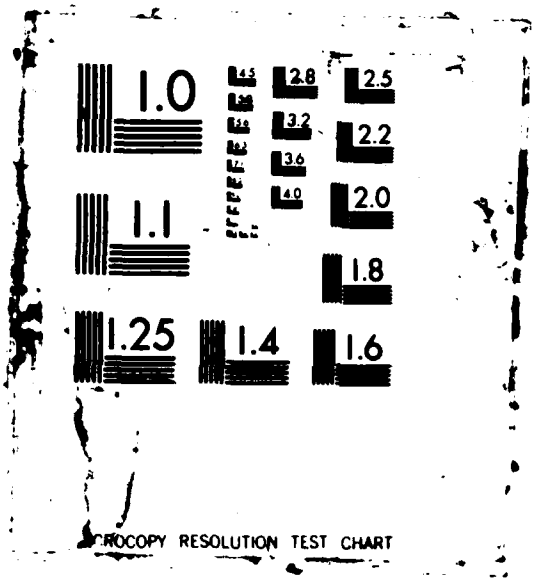
1.0
1.1
1.25
1.4
1.6
2.8
2.5
3.2
2.2
3.6
2.0
4.0
1.8
CROCOPY RESOLUTION TEST CHART

NPS67-86-004

NAVAL POSTGRADUATE SCHOOL

Monterey, California

GAS TURBINE COMBUSTOR AND
ENGINE AUGMENTOR TUBE SOOTING
CHARACTERISTICS

J. S. BENNETT, C. H. JWAY, D. J. URICH

AND

D. W. NETZER

DECEMBER, 1986

Prepared for: Naval Air Propulsion Center
Trenton, New Jersey 08628-0176

DISCLAIMER NOTICE

THIS DOCUMENT IS BEST QUALITY PRACTICABLE. THE COPY FURNISHED TO DTIC CONTAINED A SIGNIFICANT NUMBER OF PAGES WHICH DO NOT REPRODUCE LEGIBLY.

SECURITY CLASSIFICATION OF THIS PAGE

A179 423

REPORT DOCUMENTATION PAGE

1a REPORT SECURITY CLASSIFICATION UNCLASSIFIED	1b RESTRICTIVE MARKINGS
2a SECURITY CLASSIFICATION AUTHORITY	3 DISTRIBUTION AVAILABILITY OF REPORT
2b DECLASSIFICATION / DOWNGRADING SCHEDULE	
4 PERFORMING ORGANIZATION REPORT NUMBER(S) NPS67-86-004	5 MONITORING ORGANIZATION REPORT NUMBER(S)
6a NAME OF PERFORMING ORGANIZATION Naval Postgraduate School	6b OFFICE SYMBOL (If applicable)
6c ADDRESS (City, State, and ZIP Code) Monterey, CA 93943	7a NAME OF MONITORING ORGANIZATION
8a NAME OF FUNDING/SPONSORING ORGANIZATION Naval Air Propulsion Center	8b OFFICE SYMBOL (If applicable)
8c ADDRESS (City, State, and ZIP Code) Trenton, NJ	7b ADDRESS (City, State, and ZIP Code)
	9 PROCUREMENT INSTRUMENT IDENTIFICATION NUMBER N6237686WR 00013
	10 SOURCE OF FUNDING NUMBERS

PROGRAM ELEMENT NO	PROJECT NO	TASK NO	WORK UNIT ACCESSION NO

11 TITLE (Include Security Classification)

Gas Turbine Combustor and Engine Augmentor Tube Sooting Characteristics

12 PERSONAL AUTHOR(S)

J.S. Bennett, C.H. Jway, D.J. Urich and D.W. Netzer

13a TYPE OF REPORT	13b TIME COVERED	14 DATE OF REPORT (Year, Month, Day)	15 PAGE COUNT
Final	FROM Oct 85 TO Sept 86	Dec 1986	85

16 SUPPLEMENTARY NOTATION

17 COSATI CODES			18 SUBJECT TERMS (Continue on reverse if necessary and identify by block number)
FIELD	GROUP	SUB-GROUP	

19 ABSTRACT (Continue on reverse if necessary and identify by block number)

An experimental investigation was conducted to investigate the effects of smoke-suppressant fuel additives, fuel composition and combustor operating environment on the soot characteristics within the combustor and across an engine exhaust augmentor tube. A T63 combustor was used with fuel additive pumps and an exhaust augmentor tube. Soot mean diameters and concentrations were measured at two locations within the combustor and at the exhaust of the augmentor tube using three-wavelength light transmission and multiple-angle forward scattering measurements and collection probes. Fuel and air flow rates were varied and combustor inlet air temperature was varied using a hydrogen-fueled vitiated air heater.

Combustor flow conditions were found to significantly change soot characteristics as well as the effects of smoke-suppressant fuel additives. D_{32} varied between 0.10 and 0.30 microns within the combustor. D_{32} increased significantly across the engine augmentor tube, to sizes as large as 0.43 microns.

20 DISTRIBUTION/AVAILABILITY OF ABSTRACT	21 ABSTRACT SECURITY CLASSIFICATION
☒ UNCLASSIFIED/UNLIMITED ☐ SAME AS RPT ☐ DTIC USERS	
22a NAME OF RESPONSIBLE INDIVIDUAL	22b TELEPHONE (Include Area Code) / 22c OFFICE SYMBOL

DD FORM 1473, 84 MAR 83 APR edition may be used until exhausted
All other editions are obsolete

SECURITY CLASSIFICATION OF THIS PAGE

☆ U.S. Government Printing Office 1986—606-24

TABLE OF CONTENTS

LIST OF TABLES

LIST OF FIGURES

NOMENCLATURE

a	Constant in upper limit distribution function, 1.13
A	Cross-sectional area of particle
AR	Augmentor tube augmentation ratio, $\dot{m}$ pumped/$\dot{m}$ combustor
CH	Cerium Hex-cem
d,D	Particle diameter
D_m	Maximum particle diameter
D_{32}	Volume-to-surface mean diameter
F	Fuel-to-air ratio, Fraunhofer function
Fer	Ferrocene
g_e	32.2 lbm-ft/lbf-sec^2
I	Intensity
J_1	Besel function of order 1
L	Path length containing particles
m	Index of refraction of particles
$\dot{m}$	Mass flowrate
M	Mach number
N	Number concentration of particles
P,P_s	Static pressure
P_t	Stagnation pressure
Q	Dimensionless extinction coefficient
$\bar{Q}$	Average dimensionless extinction coefficient for polydispersion
R	Gas constant
S	Exhaust nozzle - augmentor spacing
T	Temperature, transmittance
T_t	Stagnation temperature
V	Velocity

α Particle size parameter, $\pi D_m/\lambda$

γ Ratio of specific heats

δ Constant in upper limit distribution function, 1.26

θ Scattering angle

λ Wavelength

ξ D/D_m

ρ Density of particle

σ Standard deviation of particle size distribution

I. INTRODUCTION AND OVERVIEW

The mechanism of soot formation in modern gas turbine aircraft engine combustors is of great interest since soot production is a factor affecting not only aircraft engine life and reliability, and aircraft combat survivability, but also atmospheric pollution levels and overall visibility. All current high performance gas turbine engines produce enough soot during some phase of operation to pose a problem for both designers and users.

The maintenance of high performace turbofan/turbojet engines by the U.S. Navy/Air Force is carried out in test cells on shore based facilities. These test cells are required to adhere to regulations and guidelines set down by the Environmental Protection Agency regarding emission of air pollutants. In addition to these federal regulations, local state laws often impose more stringent requirements to curb pollution. These regulations are applicable only while the engine is being tested on the ground, but not when the engine is airborne. Therefore, although reduction of in-flight pollutants is a long term goal, the primary immediate concern is the control of exhaust products that an engine generates in a post-overhaul test conducted in a test cell.

To comply with the emission regulations existing test cells can be modified to treat the exhaust products from the engine under test. However, this is extremely costly. Another, less expensive alternative is to modify the fuel itself, or the combustion process, so that cleaner exhaust products are produced.

As a short term solution to this problem, various fuel additives have been developed which in some way reduce soot concentration and/or visibility. Use of these additives to meet local air quality standards is economically

feasible when running engines for short periods in test cells. However, design of a soot-free engine would be a better long term solution. The complex processes which occur during combustion in these engines need further investigation to help define the role of additives and fuel composition in soot formation.

Few new test cells are being constructed. Therefore, the existing test cells are being required to meet tighter constraints in both noise and pollutant emissions while engine types and size are changing. Methods for the initial design and subsequent modifications, as well as the design of pollution/noise abatement equipment, would be facilitated if accurate prediction capabilities for inlet air and exhaust flowfields were readily available. Current test cells use augmentor tubes (ejectors) to prevent engine exhaust gas recirculation and reduce the temperature as well as to suppress noise.

Temperature, pressure and velocity distributions in augmentor tubes, if known, could be used to help determine materials required in construction, dimensions required for strength and adequacy of flow, and the effects of pollution/noise control devices inserted or injected into the flow.

The overall objective of the present effort at the Naval Postgraduate School has been to experimentally investigate the working mechanisms of smoke suppressant fuel additives and the effects of the additives, and fuel composition on (1) combustor and augmentor tube exhaust opacity, (2) particle size and concentration and temperature distribution within the combustor, and (3) particle size and concentration changes across a test cell augmentor tube.

The experimental apparatus is currently based on a T63 combustor with

fuel additive pumps and an aft pressure enclosure. The combustor employs an exhaust nozzle which exhausts into an augmentor tube. Soot mean diameters and concentrations are measured in the combustor, in the aft pressure enclosure and at the exit of the augmentor tube using three-wavelength light transmission measurements and multiple-angle forward light scattering measurements. Collection probes are also used. Variable combustor inlet air temperature is provided with a hydrogen-fueled vitiated air heater.

The three-wavelength light transmission measurement technique can be used to very low transmittance values and yields the mean (D_{32}) particle size and concentration. It does not yield particle size distribution data. Rather, it requires an assumed distribution together with knowledge of the index of refraction. The practical range of measurement for visible light is approximately 0.05 to 0.40 microns. The light scattering technique is generally able to determine particle size for particles larger than 0.05 microns. The two techniques can be used together to obtain D_{32}, the "apparent" particle index of refraction, and the particle concentration.

In general, D_{32} has been measured in the range of 0.15 to 0.25 microns. A value of D_{32} of 0.15 microns would yield an arithmetric mean diameter of approximately 0.07 microns. Collected exhaust products also show many particles in this size range, but is is not known whether or not these "large" soot particles are the result of the collection process.

An initial test series was conducted (Ref. 1) with the combustor operating at design air and fuel flowrates and design pressure with the following major results:

(1) Additives increased soot size without effecting mass concentration.

(2) Additives were less effective with lower combustor air inlet temperature.

(3) Exhaust D_{32} was independent of fuel composition and fuel-air ratio.

(4) A soot mean index of refraction of 1.95 - 0.66i resulted in the best data correlation for the light transmission measurements.

The primary test series conducted in the present investigation was made at the same pressures and fuel-air ratios as the initial study, but with reduced flowrates. Thus, the fuel atomizer was operating at less than design pressure drop (poorer atomization and fuel distribution) and the air mixing rates (primary zone fuel-air ratio) were modified.

Earlier experimentation on augmentor tubes conducted in a Naval Air Rework Facility, Alameda, California test cell by Mallon, Hickey and Metzer (Ref. 2) showed the viability of computer simulation of the test cell flow field as well as the types of difficulties that can occur in acquiring data for model validation in actual engine testing. The latter resulted from the severe temperature and pressure conditions to which the full scale testing subjected the instrumentation.

It is important to understand the processes that occur within the augmentor tube if effective controls of test cell exhaust stack emissions are to be implemented. A major question that needs to be answered is, what effects do engine operating conditions (exhaust temperature, soot characteristics, Mach number, etc.) and augmentor design have on the changes in soot size and soot and gaseous emission concentrations across the augmentor tube?

The augmentor tube used in the prevent investigation was instrumented

for flowfield determinations (temperature, pressure and velocity), as well as for the measurement of particle size variations. Operating variables investigated included changes in augmentation air ratio, combustor air inlet temperature, fuel composition and fuel additives. A further goal was to provide data for initial validation of a computer code for the augmentor tube flowfield.

II. EXPERIMENTAL APPARATUS

A. GENERAL DESCRIPTION

A summary of the test apparatus is presental below.

(1) A T63-A-5A gas turbine combustor with fuel additive pumps and aft pressure enclosure.

(2) An Augmentor tube placed at the exit plane of the 'engine' exhaust nozzle.

(3) Soot mean diameter and concentration measured in combustor, in aft pressure enclosure and across the augmentor tube using:

- 3-wavelength light transmission measurements,
- 2 and 3-angle light scattering measurements,
- Water cooled collection probes with scanning electron microscope.

(4) NO_X and stagnation temperatures measured with probes and a gas chromatograph.

(5) Augmentor tube velocity, temperature and pressure profiles measured for comparison with 3-D elliptic computer code predictions.

(6) Hydrogen fueled vitiated air heater with oxygen make-up used to provide variable combustor inlet air temperatures.

B. COMBUSTOR

An Allison T-63-A-5A combustor can was used. Included were the ignitor, combustor housing, liner and turbine nozzle block. A stainless steel chamber was attached behind the nozzle block with a converging exhaust nozzle sized to provide the proper chamber pressure. Figure 1 is a schematic of the combustor and figure 2 presents photographs of the combustor on the test stand.

C. AIR AND FUEL SUPPLIES

Compressed air for the combustor was supplied from a 3000 psi storage tank system. Air flowed through several valves and piping to enter the combustor through two ducts which originally received air from the engine's compressor. Remote control for air flowrate was achieved using a dome loaded pressure regulator and sonic choke. A solenoid operated valve controlled on/off operation. Air pressure and temperature were monitored at the sonic choke, allowing calculation of air flowrate.

A 20 gallon tank supplied pressurized fuel through a turbine flowmeter, a throttle valve and an electric solenoid shutoff valve. Nitrogen, remotely controlled by a dome loaded regulator, was used to set the desired fuel tank pressure. Figure 3 is a schematic of the air and fuel supply systems.

D. HYDROGEN-FUELED VITIATED AIR HEATER

A vitiated air heater was installed downstream of the inlet air sonic choke. Make-up oxygen was added to the heated inlet air prior to entering the combustor to account for the oxygen burned with the hydrogen. Ignitor and heater gas controls were located in the control room. A thermocouple was used

to measure the heater outlet (combustor inlet) air temperature.

E. COMBUSTOR THERMOCOUPLES

Five thermocouple stations were located radially in the combustor (Figs. 4,5). Chromel-alumel thermocouple outputs were recorded by the data acquisition system.

F. ADDITIVE METERING PUMPS

Two Eldex Model E precision metering pumps controlled the fuel additive flowrates and were remotely operated by a switch in the control room. Additive volume used was determined by measuring the amount of liquid in the reservoirs before and after pump operation. Mixing of additive and fuel was done by a swirl-type mixer.

G. CONTROLS AND DATA RECORDING

All data were recorded by a Hewlett-Packard data acquisition system. Pressures, temperatures and fuel flowrates along with transmittance and scattering diode voltages were recorded for each phase of a run. Real time exhaust temperature was displayed on a strip chart recorder for determination of attainment of steady-state operation.

Each run consisted of four phases: pre-ignition data, hot run data with and without additives, and post-fire data. For each phase, desired parameters were monitored and recorded and certain test sequences were controlled by the data acquisition system. Upon completion of each test, a hard copy of the desired parameters was produced.

H. COMBUSTOR PARTICLE SIZE DIAGNOSTICS

A schematic of the combustor instrumentation is shown in figure 6. Details and dimensions of the light scattering and light transmission apparatus are presented in figures 7, 8, 9, and 10. Several variations to those presented in the figures were employed. Later tests were conducted with the white light source used in the combustor section replaced with a He-Ne and an Argon-ion laser.

In this investigation, a combination of light transmission and forward light scattering techniques was utilized to measure the particle size D_{32} and the mass concentration (Cm). The D_{32} determined from light scattering measurements served as a check on the value determined from the light transmission measurements to increase confidence in the data.

In the exhaust region of the combustor, white-light from a tungsten source traveled through the test section to the detector assembly, where the beam was split into three parts, each passing through a narrow-pass interference filter to a photodetector. The transmission measurements from these three wavelengths produced three values of mean extinction coefficient ratios. From plots of mean extinction coefficient ratio versus D_{32} for different indices of refraction for the soot particles, it was possible to determine D_{32} and the index of refraction of the particles. At the same time, scattered light from a He-Ne laser was measured at 20° and 40° in the exhaust region. With the intensity ratio (multiplied by the sin 40°/sin 20° to compensate for the difference in scattering volume at the two angles) as input to a plot of intensity ratio versus D_{32}, a second measurement of D_{32} was obtained. This value was independent of the refraction index of the particle and was also independent of the light transmission measurements.

In the combustion region, two laser sources were used for the light transmission measurement. This yielded one mean extinction coefficient ratio. With the index of refraction determined from the three-wavelength measurement in the exhaust region and this single ratio, the plot of mean extinction coefficient ratio versus D_{32} gave the value of D_{32} in the combustion region. It was assumed that the index of refraction of the particles remained unchanged as it passed from the combustion region to the exhaust region. Scattered light measurements were to be taken at 20° and 40° for the He-Ne laser source to yield a second value or D_{32} as a check against that obtained by the two-laser transmission measurements. However, these scattering measurements could not be successfully taken because of the presence of excessive combustion light and the low output power of the He-Ne laser. Finally, from the value of D_{32} obtained from the two-laser measurement, the mass concentration was computed.

In initial tests using a white-light source in the combustor optical path, phase-lock amplifiers were unsuccessful in separating the signals from the source and from the combustion generated light. Therefore, tests were conducted using a source "light-on" and then "light-off" technique to obtain the transmittance values at three wavelengths. This method was partially successful, but was limited in accuracy due to the magnitude of the combustion generated light. The projector light source was then replaced by 2 lasers, an argon laser operating at .488 microns and a He-Ne laser operating at .6328 microns. These sources, being significantly more intense, were able to be detected through the smoke cloud despite the combustion light. The light chopper, operating at 90 Hz, was placed in the laser path before entering the combustor. The photodiode detector outputs (containing both the combustor and laser light) were passed through a phase-lock amplifier which was

synchronized with the chopper. The phase lock amplifier produced an output which was proportional to the chopped light signal. In addition, laser line filters were installed in the photodiode detectors to help filter out combustion light. Before actual data were taken, several trial tests to evaluate the effectiveness of this setup were carried out and the results showed that the combination of light chopper, phase lock amplifier and laser line filters did eliminate the influence of combustion light on the transmittance readings.

As the problem of combustion light interfering with the transmittance measurement did not exist in the exhaust region, a projector-type light source was used here. The transmitted light entered the photodiode detector box and was split into three paths by beam splitters. These three beams were collected individually by three photodiodes which had filters of .450, .650 and 1.014 microns respectively. For light scattering measurements in the exhaust region, a He-Ne laser beam at .6328 microns was used and the phodiode detectors were positioned at 20° and 40° to collect the scattered light.

I. AUGMENTOR TUBE AND INSTRUMENTATION

The augmentor tube, shown in figures 11 and 12, was instrumented at stations 1.3 inches inside the bell mouth and 14.0 inches inside the exhaust end. Allowances for adjustment in the axial positioning of the tube and the use of different inlet geometries enabled different augmentation ratios to be obtained.

The optical measurement apparatus (Fig. 13), which included a three-wavelength light transmission device and a two-angle, forward scattering light intensity device, were cart-mounted and positioned immediately aft of

the augmentor tube. Each of these optical devices provided a measurement of the mean soot particle diameter (D_{32}).

The augmentor tube (Fig. 14), through viscous mixing of the primary jet exhaust from the T-63 with the ambient air, entrains a mass flow such that at the augmentor exhaust, the mass flow is greater than that of the primary jet. If a sufficient length of tube is provided, the velocity (and temperature) profile at the augmentor exhaust will appear relatively flat and considerably reduced in peak magnitude. It is by this means that the exhausts of gas turbine engines are conditioned before entering a test cell exhaust stack.

For determination of the mass flow through the augmentor tube, pressures and temperatures at various tube positions had to be made. Two methods were used.

The first was an electric motor driven traversing probe (Fig. 15), which yielded stagnation pressure, stagnation temperature and static pressure. The probe, which consisted of a United Sensor KT-18-C/A-12-C Kiel probe enclosed within a 0.375 inch stainless steel tube, and a static pressure probe extension, was installed 1.3 inches inside the bellmouth of the augmentor tube.

The second method of data generation was a stationary stagnation pressure (X-shaped) rake attached 14.0 inches inside the exhaust end of the augmentor tube (Fig. 16).

In the bypass-air region of the augmentor tube inlet flow, and in the augmentor tube exhaust flow, the gas was assumed to be ideal and incompressible since the air flow in these regions had very low velocity

($M << 1.0$). Thus, the velocity was determined using:

$$V = [2(P_t - P_s)RT/P_s]^{1/2} \quad (1)$$

Within the central core of the augmentor inlet flow, the flow was near-sonic due to underexpansion of the choked T-63 exhaust nozzle. In this region compressibility effects could not be ignored and the velocity was determined as follows:

$$V = M\{\delta q_c RT\}^{1/2} \quad (2)$$

Since γ varies somewhat with temperature, the measured stagnation temperature was used to estimate its value for pure air. The lean overall fuel-air ratio did not warrant any corrections for gas composition change. The local Mach numbers were determined using:

$$M = \{[2/(\gamma-1)][P_t/P_s)^{(\gamma-1)/\gamma} - 1]\}^{1/2} \quad (3)$$

Similarly, the static temperature was determined by:

$$T = T_t/\{1 - [(\gamma-1)/2]M^2\} \quad (4)$$

Calculation of γ was done by using a polynomial fit developed by Andrews and Biblarz [Ref. 3].

III. PARTICULATE SIZING METHODS

A. LIGHT TRANSMISSION TECHNIQUE

K. L. Cashdollar [Ref. 4] has successfully applied this technique to measure the particle size and mass concentration of a cloud of smoke. The transmission of light through a cloud of uniform particles is given by Bouguer's Law (Ref. 4]:

$$T = \exp(-QAnL) = \exp[-(3QC_mL/2\rho d)] \quad (5)$$

A more useful relationship was developed by Dobbins [Ref. 5] for a polydisperse system of particles:

$$T = \exp[-(3\bar{Q}C_mL/2\rho D_{32})] \quad (6)$$

Using Mie scattering theory, $\bar{Q}$ can be calculated as a function of particle size, wavelength of light, complex refractive index of the particle relative to the medium and the standard deviation of the particle size distribution. A log-normal distribution for the smoke particles was assumed. A computer program (provided by K.L. Cashdollar of the Pittsburgh Mining and Safety Research Center, Bureau of Mines) produced plots of $\bar{Q}_\lambda$ and $\bar{Q}_\lambda$ ratios (which are both functions of wavelength) versus values of D_{32}. Taking the natural logarithm of equation 6 and writing it for a specific wavelength:

$$\ln T_\lambda = \bar{Q}_\lambda [-3C_mL/2\rho D_{32}] \quad (7)$$

Since the three-wavelength detector measures the transmission for all three wavelengths over an identical path through the smoke cloud, the ratio of the logarithms of the transmissions at any two wavelengths is equal to the ratio of the calculated extinction coefficients for the same wavelengths:

$$[\ln T_{\lambda 1}/\ln T_{\lambda 2}] = [\bar{Q}_{\lambda 1}/\bar{Q}_{\lambda 2}] \qquad (8)$$

With this ratio as the input parameter to the $\bar{Q}_\lambda$ ratio versus D_{32} plot, the value of D_{32} can be determined. As the three wavelength measurements yield three ratios, three values of D_{32} will be obtained. If the refractive index (m) and the size distribution width (σ) are correctly chosen, all three values of D_{32} obtained from the $\bar{Q}_\lambda$ versus D_{32} plots will be consistent. If the three values of D_{32} are not consistent, either the size of the distribution width or the refractive index, or both, must be varied. Most of the particulates from the combustion can reasonably be assumed to be carbon. From previous studies [Ref. 4], some refractive indices for carbon are available. In this investigation a complex refractive index of $m = 1.95 - i0.66$ was most often successful in correlating the data. The refractive index of the surrounding medium was unity for air and the standard deviation of the particle distribution, σ, was taken as 1.5. Other values that have been used with less success are $m = 1.80 - .60i$, $1.90 - .35i$, $1.95 - 66i$, $1.60 - .60i$, and $\sigma = 2.0$. Once $\bar{Q}_\lambda$, D_{32}, and T_λ are known, the mass concentration can be calculated from the following rearrangement of equation 7:

$$C_m = -[2\rho D_{32} \ln T_\lambda]/3\bar{Q}_\lambda L \qquad (9)$$

Figures 17 to 20 show typical plots produced by the Cashdollar program for given values of refraction index (m) and three values of wavelength.

The three-wavelength light transmission measurement method has the advantages that (1) it can be used to very low transmittance values and still yield accurate mean particle size and concentration, (2) it requires only inexpensive apparatus, and (3) data reduction is simple. However, (1) it generally only yields mean particle size with no information on the size distribution, (2) it is generally limited to particle sizes between approximately 0.05 and 0.4 microns, (3) it requires knowledge of the index of refraction, and (4) it assumes that the particle index of refraction is independent of wavelength.

B. FORWARD LIGHT SCATTERING TECHNIQUE

An alternative or supplement to the light transmission technique for finding D_{32} is to measure scattered light. For large particles $\alpha \left(= \frac{\pi D}{\lambda}\right) > 5$ it has been shown that using only Fraunhofer diffraction can result in accurate particle size determination. In fact, Hodkinson [Ref. 6] has shown that by using the ratio of intensities at two forward angles, particles can be sized down to values of $\alpha \approx 1.0$ ($D \approx 0.2$ microns for $\lambda = .6328$ microns) using only Fraunhofer diffraction. Boron & Waldie [Ref. 7] have shown that accuracy rapidly decays for $D < 0.5$ microns if only two angles are employed. Powell, et. al., [Ref. 9] have successfully used the technique for $D_{32} \approx 0.4$ microns. Making measurements with more than one pair of forward scattering angles can reveal the accuracy of measurement [Ref. 6]. Polydispersions are also less prone to measurement errors for D_{32}. Of course, if the more complex Mie functions are used, then there is much less uncertainity in the measurements.

Following the method of Dobbins, et al. [Ref. 8] and Powell, et. al. [Ref. 9] for the Fraunhofer forward lobe

$$\frac{I(\theta_1)}{I(\theta_2)} = \frac{F(\theta_1)}{F(\theta_2)}$$

Powell and Zin [Ref. 9] assumed an upper-limit-distribution-function (ULDF) as proposed by Mugele & Evans [Ref. 10], which gives the following equation for $F(\theta)$:

$$F(\theta) = \int_0^1 (1+\cos^2\theta)[J_1(\alpha\theta\xi)/\theta\xi]^2 \times \exp[-(\delta \ln(a\xi/1-\xi))^2]d\xi/1-\xi \qquad (11)$$

where

$$\alpha = \pi D_m/\lambda \qquad (12)$$

$$D_m/D_{32} = 1 + a\exp(1/4\delta^2) \qquad (13)$$

and a and δ are adjustable parameters. Typical values of a and δ are 1.13 and 1.26 as given by reference 9.

The ratio of scattered light intensities at two forward angles is relatively insensitive to particle refractive index and concentration. This is a consequence of the forward lobe being primarily due to Fraunhofer diffraction phenomena, which are independent of optical properties of the particle (since diffraction arises from light passing near the particle rather than light undergoing reflection or refraction) [Ref. 9]. For given

values of α , angle θ , a and δ , equation 11 is readily evaluated by numerical integration, producing a plot of intensity ratio versus D_{32} . In this investigation, intensity measurements at 20° and 40° were taken. In order to have the recorded intensities referenced to the same scattering volume, the intensities must be multiplied by sin θ . The ratio of the intensity at 40° multiplied by sin 40° to the intensity at 20° multiplied by sin 20° is then used for entry to the plot, yielding a value of D_{32} . Figure 21 shows a typical plot of the intensity ratio versus D_{32} for a wavelength of .6328 microns.

Currently, plots similar to Figure 21 are being developed for 40°/20°, 40°/10°, and 20°/10° based upon both Fraunhofer diffraction and the more complete Mie functions [Ref. 11].

C. COMBINATION TECHNIQUES

Using both forward scattering measurements (at two or more angles) and transmittance measurements at three wavelengths simultaneously can increase the accuracies of measurement for particle size and concentration. One such technique is shown in Figure 22. Light scattering measurements are used to yield D_{32}, independent of index of refraction (for $D > 0.3$ microns) and concentration. In this case, the light transmission measurements yield the standard deviation of the assumed distribution and the "effective" particle index of refraction. The extinction-coefficient and measured transmittance at one wavelength then yield the particle concentration.

The term "effective" particle index of refraction is used in contrast to the value for the pure substance. The former is what the optical technique "sees." As found by Powell & Zinn [Ref. 9] (and others) soot agglomerates may

be quite porous and have an "effective" index of refraction significantly less than that for a solid carbon particle.

Unfortunately, soot sizes produced by gas turbine engines have ranged from 0.01 to 1.0 microns. When $D \leq 0.3$ microns, D_{32} becomes a function of both the scattered intensity ratio and the particle index of refraction (Mie scattering vs. Fraunhofer diffraction). In this case another iteration step is required to determine D_{32} , m , and σ .

IV. RESULTS AND DISCUSSION

A. INITIAL TESTS AT NOMINAL COMBUSTOR FLOWRATE

The initial tests in the current investigation were conducted at the same test conditions as in a previous investigation [Ref. 1]. The particle sizing diagnostics were improved and data acquisition and experiment control were transferred from manual operation to the computer system.

A test using NAPC fuel #1 (Table I) and the 12% Cerium Hex-Cem additive was conducted. During the run, data with an additive concentration of 20ml/gallon of fuel was taken first, followed by data without any additive. All hot-run data were taken after the combustor exhaust temperature had reached a steady state value (slightly above 1200 degrees F. for these tests). Table II summarizes the average test conditions.

Results of the light transmission measurement technique to determine average particle size are summarized in Table III. The light transmission data were correlated best with the Mie curves using a refractive index of 1.95 -.66i and a standard deviation of 1.5.

Light transmission particle size data was improved over previous results with the T-63 combustor [Ref. 1]. In general, correlation to within a range of ± .04 microns or less was obtained. Measurements in the combustion region were taken across a large recirculation zone. Thus, the measured particle size represented an average of all the particle sizes in this zone and the surrounding annulus.

In the exhaust region, the limited data indicated a significant increase in particle size when the additive was used. However, particle mass concentration (Table IV) did not change, indicating that use of the additive changed the particle size but not the total mass. This result was in agreement with the data presented in reference 1.

Results from the light scattering photodiodes in the exhaust stream are summarized in Table V. This technique also indicated that an increase in particle size occurred when the fuel additive was used, but there was a discrepancy between the particle sizes obtained from the transmitted and scattered light measurements. The scattered light measurements resulted in smaller particle diameters. This may have resulted from (1) uncertainties in the scattered data (due to the low signal strengths recorded) and/or (2) the uncertainty in ln-ratios when transmittance values are very high.

B. COMBUSTOR RESULTS AT LOW MASS FLOWS

The investigations reported in Reference 1 and above were conducted using four exhaust tubes at the aft-end of the combustor pressure vessel. This was done to facilitate the use of sampling probes which traversed the combustor centerline and were inserted from the rear of the apparatus. Subsequently, the tubes were removed and a converging nozzle was added. This

was done to provide realistic input into the augmentor tube, which was to be positioned downstream of the "engine".

The current investigation was conducted at the same fuel-air ratios and combustion pressures as in the earlier investigations (Ref. 1 and above), but with lower air and fuel flowrates. These conditions resulted in lower fuel flowrate through the atomizer and lower air flowrate through the combustor can mixing and dilution holes. Thus, it was expected that the results would more nearly correspond to operating conditions (idle, etc.) in which the fuel atomization was not optimum and in which the primary zone fuel-air ratio would be altered.

In this investigation, NAPC #7 fuel was tested at fuel-air ratios between .014 and .016. In addition, the effects of three smoke suppressant fuel additives (Ferrocene, 12% Cerium Hex-Cem and USLAD 2055) were tested using the NAPC #7 fuel. Two tests were also carried out using NAPC #3 fuel. The properties of NAPC #3 and #7 fuels are shown in Table I. Fuel #7 was higher in aromatic content and lower in hydrogen than fuel #3. Fuel additive and fuel-air ratio effects on mean soot diameter, soot concentration, and opacity are discussed below.

Attempts to use the phase-lock amplifiers/light choppers with the low intensity white-light source were not successful in the combustor. The combustor generated light was very intense across the visible spectrum, resulting in an inability to separate the transmitted light and combustor light signals. For this reason, two lasers were employed with wavelengths of .488 and .6328 microns. These provided sufficient intensity for the phase-lock amplifiers to successfully remove the random frequency combustion light. However, only two wavelengths were used. This did not permit

determination of the index of refraction for the particles (as possible when three wavelengths are used). It was therefore assumed that the index of refraction was unchanged from the value determined in the aft pressure vessel, where the white light could be successfully used since there was no significant radiation of visible light.

Runs #4, 5, 7, 8, and 10 yielded D_{32} values with a large uncertainty, even though the transmittance values were steady (Table VI).

Run #10 did not provide a D_{32} value for the combustion region. This was because the extinction coefficient ratio obtained from the experiment resulted in a value off of the curve of the extinction coefficient ratio versus D_{32} plot.

Runs #11 and #12 gave good exhaust transmittance readings, but the computed extinction coefficient ratios did not result in proper values for entry into the plots to obtain a D_{32} value. In the earlier experiments at nominal fuel and air flowrates, the uncertainty in D_{32} was generally as low as the best data obtained currently. There are at least two possible causes for this "lack-of-correlation" of the particle size data. If the particle size distribution was bi-modal, then the assumed mono-modal, log-normal distribution would result in unrealistic Mie predictions. Powell and Zinn [Ref. 12] have also reported that soot particle porosity can result in a significantly reduced "effective" particle index of refraction.

Thus, a shift in atomization and mixing conditions appears to have significantly changed the soot particle characteristics.

D_{32} is plotted against fuel-air ratio in figure 23 and vs. exhaust temperature in figure 24. D_{32} is seen to increase with increasing

fuel-air ratio. It also is observed (although the data is limited to one test) that an increased combustor air inlet temperature resulted in a decreased D_{32} at the same fuel-air ratio. However, as seen in figure 24, D_{32} correlates with exhaust temperature, independent of air inlet temperature. As expected, increased inlet air temperature increased the exhaust temperature (at a given fuel-air ratio) (see fig. 25) and the latter appears to have the dominant effect on D_{32}.

Using NAPC #3 fuel (lower aromatics and higher hydrogen content) in place of NAPC #7 resulted in larger D_{32} at the same fuel-air ratio. NPAC #3 also produced a lower exhaust temperature for the same fuel-air ratio. Thus, larger D_{32} was expected. However, even at the same exhaust temperature a larger D_{32} was observed. This result indicates that small changes in fuel composition can have effects on the mean soot size.

Transmittance (without additives) is plotted against exhaust temperature in figure 26 for the three wavelengths which were utilized. At any given wavelength, transmittance increased only slightly with exhaust temperature. This resulted (Table VII) in only small (less than 5%) changes in soot mass concentration with significant (approximately 30%) changes in D_{32}. It appears for this particular combustor and test conditions that fuel-air ratio effects soot size, but not total mass.

Figure 23 and Table VII also indicate that the use of smoke-suppressant fuel additives:

(1) had insignificant effects on exhaust temperature (heat content)

(2) increased transmittance with soot mean diameter remaining approximately constant, and

(3) reduced exhaust soot concentration (and exhaust opacity).

Comparison of figures 24 and 27 shows that in the combustor, particle size changed more rapidly with fuel-air ratio (or exhaust temperature). At low fuel-air ratios (or exhaust temperature) the particle size in the combustor and in the exhaust duct were nearly identical. As the fuel-air ratio was increased, the combustor particle diameter decreased more rapidly than in the exhaust duct. Thus, there was a growth in mean particle diameter from the combustor to the exhaust duct at higher fuel-air ratios.

The above results, which were obtained at reduced fuel and air flowrates, were considerably different than the results reported in reference 1 for nominal combustor flowrates. The major differences were as follows:

(1) Three-wavelength technique data often did not result in consistent values of D_{32}, indicating a possible bi-modal size distribution and/or a very low "effective" index of refraction, as is apparently characteristic for porous soot agglomerates.

(2) Higher aromatic/lower hydrogen fuels resulted in slightly smaller D_{32} at the same exhaust temperature and higher exhaust temperature at the same fuel-air ratio.

(3) Additives had no effect on D_{32} but reduced soot concentration.

(4) D_{32} decreased with increasing fuel-air ratio.

The data indicate that combustor test conditions (atomization and primary zone fuel-air ratio) can significantly alter exhaust soot structure and/or size distribution.

In addition, the following results were obtained:

(1) D_{32} increased in the axial direction at higher fuel-air ratios, but not at lower fuel-air ratios.

(2) D_{32} in the exhaust duct depended primarily upon, and decreased with increasing values of, exhaust temperature.

(3) Smoke suppressant fuel additives were more effective in reducing opacity with higher air inlet temperatures (~10% more reduction in C_m for 270°F increase in temperature). It is not clear at this point how the increased air inlet temperature improves additive effectiveness. Increased air inlet temperature can increase both kinetic and vaporization rates and may increase the residence time at temperature.

C. AUGMENTOR TUBE MEASUREMENTS

Measurements were also made to determine the mean soot size at the exit of the augmentor tube. In addition, augmentation air flowrate was determined by knowing the combustor flowrate and measuring the total flowrate in the augmentor tube. The later was accomplished using a pitot rake near the aft-end of the augmentor tube.

Based on earlier results with a subscale test cell [Ref. 13], the D_{32} at the augmentor exhaust was expected to be less than 0.3 microns. This prompted the use of the three-wavelength transmission technique. Particle diameters at the exhaust of the augmentor tube were measured to be in the range of 0.31 to 0.42 microns, which is large for accurate measurements using the three-wavelength technique. This manifested itself as a large spread in the values of D_{32} obtained from the three transmittance ratios, a direct result of all the extinction coefficient ratios approaching unity when particles exceed 0.4 microns (see Fig. 18). A small variation in the extinction coefficient

ratio results in a large change in D_{32}.

Attempts at calibration using National Bureau of Standard 0.9 micron polystyrene beads also resulted in a wide spread, centered on .9 micron. Transmittances in the range of 85% provided the smallest spread in the calibration attempts.

The transmittances in the exhaust stream were high, approximately 95%, which prompted the utilization of a double pass of light through the augmentor exhaust stream, as well as the installation of a blocking plate at the inlet of the augmentor tube to reduce the dilution of the soot. The blocking plate resulted in an augmentation ratio of 0.53 and transmittances of approximately 89%.

As a cross-check for particle size, a two-angle (20° and 40°) forward scattering device was installed. This device provided relatively consistent particle size data. This data was in good agreement with the data obtained using the three-wavelength device, when the latter did not exhibit its characteristic spread. As a result, the light scattering measurement device appeared to provide the better data.

The traversing Kiel probe was originally designed for use in flows with less than sonic velocity. Initial utilization, however, showed regions of supersonic flow in the expansion of the underexpanded exhaust jet of the sonically choked T-63 nozzle. This invalidated the assumption that the static pressure would be relatively constant across the augmentor inlet. Modifications to the probe were then made, which included a static port extension and strengthening of the probe support. Furthermore, in actual data runs, efforts were made to ensure that the Mach number was as low as possible

to reduce measurement errors.

The velocity profiles shown in figures 28 and 29 were obtained for future validation of the computer code for augmentor tube flowfield prediction.

Table VIII presents the transmittances for the three-wavelengths, particle diameter from each extinction ratio, the scattered light intensity ratio and the corresponding particle diameter. These runs were all conducted with the T-63 exhaust nozzle flush with the augmentor tube blocking plate. The fuel used was NAPC #7. Additives used were 12% Cerium Hex-Cem, Ferrocene Solution and USLAD-2055. Table IX is provided for comparison of fuel-air ratio, temperature and augmentation effects on particle size.

In these initial tests there were insufficient temperature measurements taken throughout a given run to accurately determine the effects of augmentor exhaust temperature on particle size. However, the augmentor exhaust temperature followed the engine exhaust temperature (fixed augmentation air dilution) which was recorded continuously throughout the run.

With one excention (Run 8, 8a), the particle size appeared to increase with fuel-air ratio (Fig. 30), opposite to the combustor behavior. This was evident in Runs 9, 10, 11, 12, and 16. Runs 8 and 8a exhibited a soot "blow-out" which resulted in a wide range in measured transmittances.

Although the accuracy of the particle size measurements may result in questionable conclusions, there did seem to appear to be a small, but consistent, increase in augmentor exhaust particle size with increasing temperature. This was in contrast to a slight decrease in D_{32} at the combustor exit with increasing temperature.

All additives exhibited the same approximate effect at the augmentor tube exhaust; a very small (.02 micron), but consistent, increase in D_{32}.

The soot mass concentration should not change appreciably across the augmentor tube since temperatures were quite low. However, soot deposits on the tube walls can remove some soot from the flow. There was no consistent trend in the calculated change in C_m when the additives were used.

Only one hot combustor air inlet run was made (Runs 13, 13a), resulting in the expected increase in engine exhaust temperature at the same fuel-air ratio (compare to Runs 8, 8a). In this case D_{32} decreased at the augmentor tube exhaust. However, the engine exhaust temperature did not appear to effect agglomeration within the augmentor tube since increased combustor fuel-air ratio and increased combustor air-inlet temperature had opposite effects on D_{32} at the augmentor exit.

From Runs 8a, 9, 9a, 10, 10a, and 13, it is evident that the mean particle diameter nearly doubled from the T-63 exhaust to the augmentor tube exhaust. This could be caused by several effects; agglomeration of particles or the walls shedding of previously impacted soot (all test runs had sooted walls in the augmentor tube).

Figure 31 shows a a typical impact collected test sample. A large variation in sizes is exhibited with the largest being approximately 1.5 microns and the smallest in the submicron range. The Hitachi 265s scanning electron microscope provides good resolution; however, the carbon make-up of the particles did not lend itself to good viewing without being flashed with gold. The specimen presented in figure 31 were not coated and developed a radiance or ghostlike appearance.

In Figure 32 the specimens were gold flashed filter paper (0.2 micron pore) on which the soot was collected through a 1/4-inch sampling tube. Again, a substantial variation in particle size from submicron to larger than 1.0 micron was observed.

D_{32} is dominated by the larger particles in a distribution. Thus, the optically measured D_{32} of approximately .34-.42 microns appears to be quite realistic. However, it is not known how much agglomeration occurred in the probe.

Augmentation air had two effects on particle size in the augmentor tube. The first was that the particles appeared to approximately double in size across the augmentor, due to agglomeration or wall shedding of previously impacted soot. The second effect was an increase in the transmittance through cross dilution with secondary air. Each of these effects could be exploited for providing a reduced stack opacity in the test cell environment.

V. SUMMARY OF RESULTS AND PRESENT EFFORTS

A. SUMMARY OF RESULTS

1. At both nominal and reduced combustor mass flowrates, a particle index of refraction of 1.95-.66i most consistently resulted in the best data correlation. D_{32} values varied between 0.10 and 0.30 microns within the combustor.
2. Combustor flow conditions (atomization and/or primary zone fuel-air ratio) significantly changed the soot characteristics. This was evident by the changes that occurred when nominal flowrates were reduced.

Nominal Flowrates	Reduced Flowrates
(a) Good correlation for D_{32} using three-wavelength methods.	(a) Often poor correlation of D_{32} using three-wavelength methods.
(b) Smoke-suppressant additives increased D_{32} without significantly effecting mass concentration	(b) Smoke-suppressant additives did not change D_{32}, but reduced mass concentration.
(c) Exhaust D_{32} was independent of fuel-air ratio and fuel composition.	(c) Exhaust D_{32} decreased with increased exhaust temperature (fuel-air ratio). Fuel with lower aromatics/ higher hydrogen content yielded larger D_{32}.

3. The cause of the poor correlation of D_{32} at low flow conditions is not known. Results from other investigators suggest that bi-modal size distributions may be present and that soot porosity can significantly reduce the "effective" index of refraction of the particles.
4. At low flowrates, changing fuel-air ratio effects D_{32} but not the total mass of soot.
5. At all flow conditions, increased combustor air inlet temperature increased the effectiveness of smoke-suppressant additives in reducing opacity. Increased vaporization and kinetic rates and possible increased residence time at temperature could all help explain this result. Further effort is required to separate the source.
6. At low combustor flowrates, soot agglomeration (growth) occurred in the axial direction at the higher fuel-air ratios, but not at lower fuel-air ratios.
7. D_{32} approximately doubled across the augmentor tube to values between 0.31 and 0.43 microns without any consistent change in

mass concentration. Collected exhaust products revealed particles from less than 0.05 microns up to approximately 1.5 microns. Agglomeration in the collection probe and/or in the augmentor tube and wall collisions/shedding can all result in these large observed particles.

8. Engine exhaust temperature did not appear to affect agglomeration within the augmentor tube. Agglomeration appears to be a function of the soot characteristics leaving the engine/combustor.

The possibility of (1) soot agglomeration in probes and (2) shifting size distributions and particle index of refraction with test conditions, fuel composition and additives indicate that various optical and intrusive measurement techniques are needed in future investigations in order to help determine the "actual" soot size distribution and index of refraction.

B. PRESENT EFFORTS

1. Completing evaluation of ten fuels and four smoke suppressant additives at two fuel-air ratios and two air inlet temperatures.
2. Varying augmentor tube diameter to vary augmentation ratio.
3. Using polished stainless steel augmentor tubes to help separate effects of agglomeration from those due to wall collisions/shedding.
4. Using combination of 3-λ light transmission and 3-θ light scattering techniques to more accurately determine D_{32} and the "effective" particle index of refraction.
5. Using electron microscope to determine whether additives effect particulate composition (and, therefore, index of refraction).
6. Generating Mie scattering profiles for bi-modal distributions.

TABLE I

FUEL PROPERTIES

	NAPC #1	NAPC #3	NAPC #7
API Gravity @ 15°	38.9	41.3	35.6
Distillation (ASTM) IBP °C	163	171	193
Composition			
Aromatics (VOL %), Max	28.5	22.8	26.4
Olefin (VOL %), Max	1.79	0.75	0.86
Hydrogen Content (Wt %), Min	13.36	13.66	12.83
Aniline - Gravity Prod., Min	5360	5811	4254
Freeze Point, °C	-30	-34	-31
Viscosity @ 37.8°C, (cSt)	1.78	1.62	1.77

TABLE II

AVERAGE TEST CONDITIONS - NOMINAL COMBUSTOR FLOWRATES

Run Number.....	1	2
Additive.....	*	None
Fuel Number.....	1	1
Chamber Pressure (psia)..	88.7	89.5
Air flow (lbm/sec)	2.20	2.21
Fuel-air ratio.....	.017	.017
Additive/fuel ratio (ml/gal)	20	0
Thermocouple temperatures (deg. R)		
#1.....	2165	2144
#2.....	2825	2846
#3.....	1830	1857
#4.....	2263	2269
T exhaust.....	1673	1665

*12% Cerium Hex-Cem

TABLE III

D_{32} FROM THREE-WAVELENGTH TRANSMISSION MEASUREMENTS

NOMINAL FLOWRATES

	Combustion Region				Exhaust Region			
Run #	T(.40)	T(.51)	T(.70)	D32	T(.45)	T(.65)	T(1.0)	D32
1*	.171	.190	.227	.29	.864	.874	.897	.37
2	.171	.180	.265	.27	.839	.865	.902	.29

D32 in Microns

Refractive Index = 1.95 - .66i, Standard Deviation = 1.5

* Cerium Hex-Cem Additive Used

TABLE IV

PARTICLE MASS CONCENTRATIONS FROM TRANSMITTED LIGHT MEASUREMENTS-NOMINAL FLOWRATES

Run #	Combustion Region $\bar{D}$	Combustion Region C_m(mg/liter)	Exhaust Region $\bar{D}$	Exhaust Region C_m(mg/liter)
1*	2.70	1.2	2.73	.16
2	2.65	1.2	2.38	.16

* Cerium Hex-cem additive used

TABLE V

D_{32} FROM SCATTERED LIGHT MEASUREMENTS IN EXHAUST REGION

NOMINAL FLOWRATES

Run #	Diode voltages 20 deg.	40 deg.	Light Intensity Ratio	Average D_{32} (microns)
1**	.080	.023	.59	.32
2	.087	.032	.76	.17

** 12% Cerium Hex-Cem Additive

Calibration constant Ktr = 1.10 Volts/Unit Light Intensity

Light Intensity Ratio = Ktr * (40 deg. voltage/20 deg. voltage) * (sin 40°/sin 20°)

TABLE VI

RESULTS FROM TEXTS USING NAPC #7 AND #3** FUELS

AT LOW MASS FLOW CONDITIONS

Run no.	Exhaust Temp (°R)	f	Combustion Region Transmittance T(0.48)	T(0.63)	D_{32} (micron)	Exhaust Region Transmittance T(1.0)	T(0.65)	T(0.45)	D_{32} (micron)
1	1790	.0163	.250	.140	.17	.888	.782	.675	.170
2	1630	.0156	.247	.176	.20	.380	.727	.616	.180-.210
3	1754	.0154	.260	.136	.10	.868	.760	.671	.180-.190
4	1530	.0141	.268	.200	.21	.830	.740	.650	.180-.260
5	1530	.0140	.270	.179	.18	.847	.763	.673	.180-.230
6	1630	.0150	.204	.144	.21	.845	.750	.662	.190-.215
6a	1643	.0148	.218	.145	.19	.858	.761	.671	.185-.205
7	1635	.0154	.264	.144	.13	.847	.725	.664	.170-.220
7a	1642	.0153	.274	.151	.13	.874	.761	.709	.170-.225
8	1594	.0145	.255	.176	.19	.847	.765	.670	.180-.250
8a	1580	.0143	.281	.188	.18	.880	.810	.730	.180-.230

6a,7a - Ferrocene

8a - 12% Cerium Hex-Cem

TABLE VI (con't)

RESULTS OF TESTS ON JAPC #7 AND #3** FUELS

AT LOW MASS FLOW CONDITIONS

Run no.	Exhaust Temp (°R)	f	Combustion Region Transmittance T(0.48)	T(0.63)	D_{32} (micron)	Exhaust Region Transmittance T(1.0)	T(0.65)	T(0.45)	D_{32} (micron)
9	1635	.0154	.265	.172	.17	.852	.759	.667	.180-.200
9a	1641	.0152	.297	.187	.16	.879	.805	.728	.190-.200
10	1632	.0150	.325	.162	*	.851	.762	.670	.170-.220
10a	1640	.0149	.337	.168	*	.886	.809	.730	.180-.200
11	1664	.0156	.090	.189	.14	.845	.788	.660	*
11a	1690	.0156	.140	.240	.16	.876	.831	.715	*
12	1632	.0156	.140	.230	.18	.850	.790	.670	*
12a	1628	.0154	.165	.245	.16	.870	.830	.720	*
13	1764	.0142	.560	.350	*	.878	.774	.698	.150-.180
13a	1760	.0141	.523	.359	*	.918	.838	.790	*
14**	1669	.0171	.270	.190	.12	.853	.765	.694	.200-.240
15**	1749	.0183	.240	.190	.10	.842	.735	.668	.210-.220

9a,10a - 12% Cerium Hex-Cem

11a,12a - USLAP 2055

13a - 12% Cerium Hex-Cem

13, 13a - Inlet air temperature = 270°F

TABLE VII

PERCENTAGE CHANGES IN SOOT CONCENTRATION AND EXHAUST TRANSMITTANCES AT LOW MASS FLOW CONDITIONS

Run no.	Mass Concentration (mg/litre)	Amount of Additive Used (ml/gal)	% Reduction in Cm	% Reduction in Exhaust Transmittance		
				T(1.0)	T(.65)	T(.45)
6	.354					
6a	.347	22.8	1.9	1.5	1.41	1.36
7	.368					
7a	.309	30.0	16.0	3.2	4.9	6.7
8	.360					
8a	.270	58.0	25.0	3.9	5.9	8.9
9	.356					
9a	.279	58.0	21.6	3.2	6.0	9.1
10	.35					
10a	.28	58.0	20.0	4.1	6.2	8.9
11	—					
11a	—	—	—	3.6	5.5	8.3
12	—					
12a	—	—	—	2.3	5.1	7.4
13*	.361					
13a*	.241	58.0	34.5	4.5	8.2	13.2

* Inlet air temperature = 270°F

TABLE VIII

SUMMARY OF OPTICAL DATA - AUGMENTOR TUBE

Run Number	Additive	Transmittances T_{100}	$T_{694.3}$	T_{450}	3 Wavelength D_{32} (microns) $\frac{1000}{694.3}$	$\frac{694.3}{450}$	$\frac{1000}{450}$	Intensity Ratio I_{40}/I_{20}	Scattering D_{32} (microns)
2		.952	.944	.943	.43	.41	.42	-	-
6		.851	.848	.844	.65	.42	.52	-	-
7a	Ferrocene	.926	.923	.923	.60	.47	.54	-	-
8		.862	.860	.863	.64	.48	.57	.586	.34
8a	12% Cerium	.934	.905	.901	.27	.38	.33	.530	.38
9		.784	.854	.850	*	.42	*	.498	.40
9a	12% Cerium	.891	.896	.893	*	.42	*	.461	.43
10		.862	.862	.861	*	.47	*	.515	.39
10a	12% Cerium	.925	.926	.926	*	.47	*	.483	.41
11		.885	.887	.883	*	.40	*	.479	.42
11A	USLAD-2055	.907	.913	.913	*	.47	*	.460	.43
12		.907	.911	.913	*	.50	*	.493	.41
12a	USLAD-2055	.908	.898	.893	.46	.38	.43	.463	.43
13		.924	.963	.923	*	*	*	.618	.31
13a	12% Cerium	-	-	-	-	-	-	.478	.42
14		.918	.894	.891	.33	.41	.37	.526	.38
14a	12% Cerium	.919	.923	.896	*	.38	*	.487	.41

Fuel = NAPC #7 Augmentor to Nozzle Spacing = Flush Blanking Plate Installed
Augmentation Ratio = .53

- = NOT Collected * = No Correlation a = additive run

TABLE IX

SUMMARY OF PARTICLE SIZE DATA-AUGMENTOR TUBE

Run Number	Fuel-Air Ratio	Temperature $T_{engine\ exhaust}$	Temperature $T_{augmentor\ exhaust}$	Additive	D_{32} Engine Exhaust	D_{32} Augmentor Transmittance	D_{32} Augmentor Scattering
2	.0156	1630	1157	None	.18-.21	.41-.43	-
6	.0150	1630	1157	None	.19-.22	.42-.65	-
7a	.0153	1642	1131	Ferrocene	.17-.23	.47-.60	-
8	.0145	1594	1136	None	.18-.25	.48-.64	.34
8a	.0143	1580	1136	12% Cerium Hex	.19-.23	.27-.38	.38
9	.0154	1635	1130	None	.18-.20	* .42 *	.40
9a	.0152	1641	-	12% Cerium Hex	.19-.20	* .42 *	.43
10	.0150	1632	1121	None	.17-.22	* .47 *	.39
10a	.0149	1640	-	12% Cerium Hex	.18-.20	* .47 *	.41
11	.0156	1664	1179	None	-	* .40 *	.42
11a	.0156	1690	-	USLAD-2055	-	* .47 *	.43
12	.0156	1632	1128	None	-	* .50 *	.41
12a	.0154	1628	-	USLAD-2055	-	.38-.46	.43
13	.0142	1764	1235	None	.15-.18	-	.31
13a	.0141	1760	-	12% Cerium Hex	-	-	.42
14	.0145	1643	1088	None	.26 (scat)	.33-.41	.38
14a	.0145	1684	-	12% Cerium Hex	.17 (scat)	* .38 *	.41

Fuel NAPC #7 Augmentation Ration = .53 Augmentor Blocking Plate Installed

Scat = Engine Exhaust Scattering Technique * = No Correlation - = Not Collected

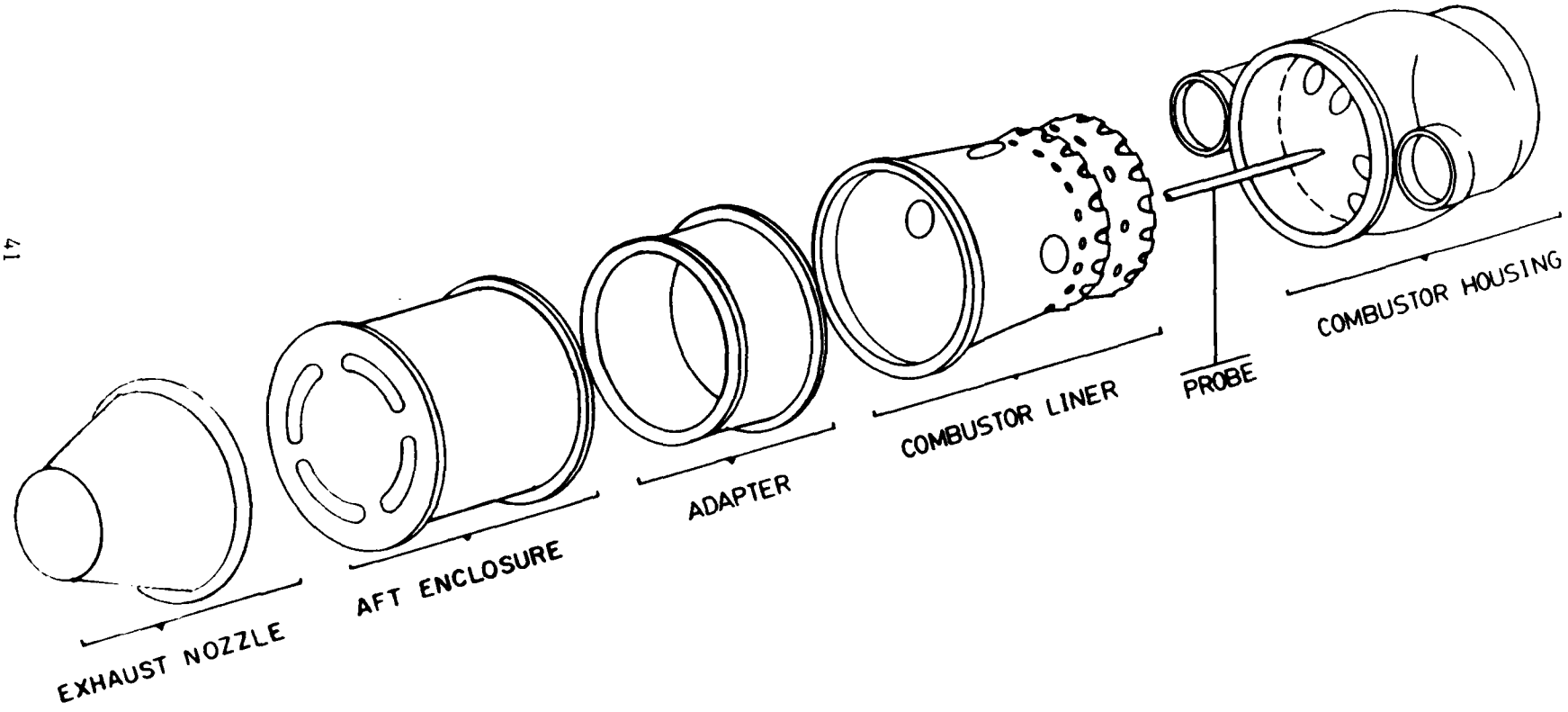

Figure 1. Schematic of T-63 Combustor Components

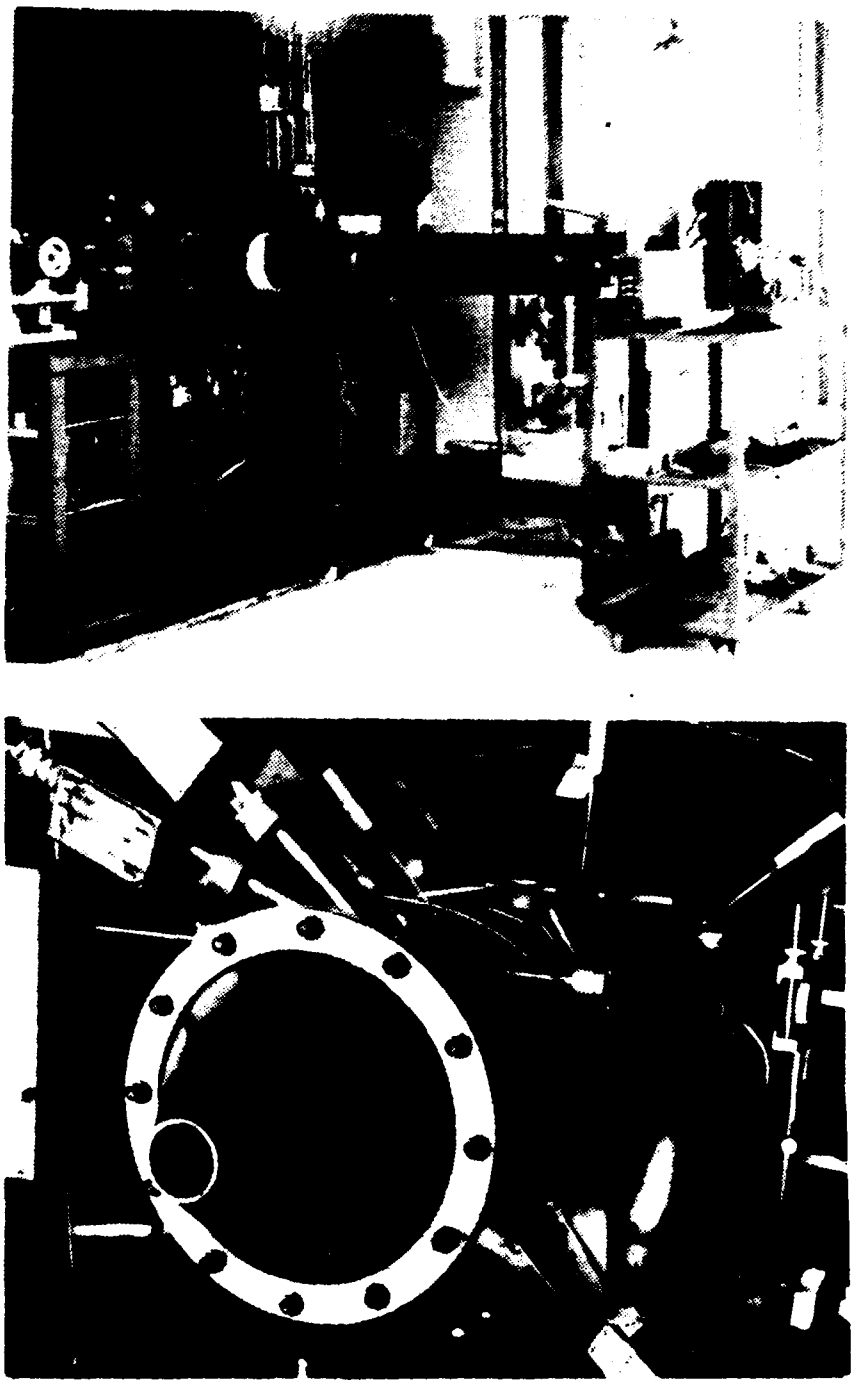

Figure 2. Photographs of T-63 Combustor Apparatus

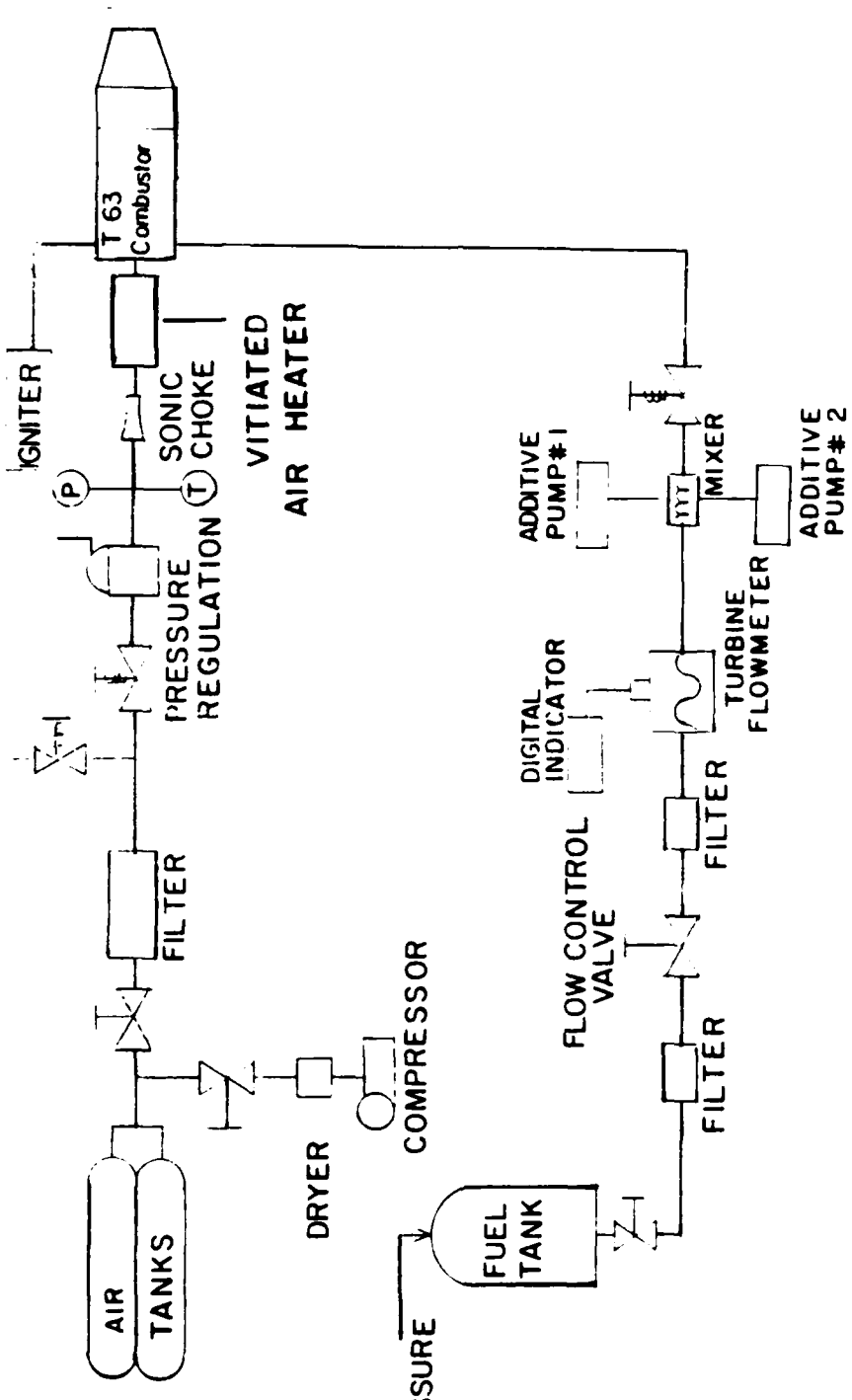

Figure 3. Schematic of Air and Fuel Supply Systems

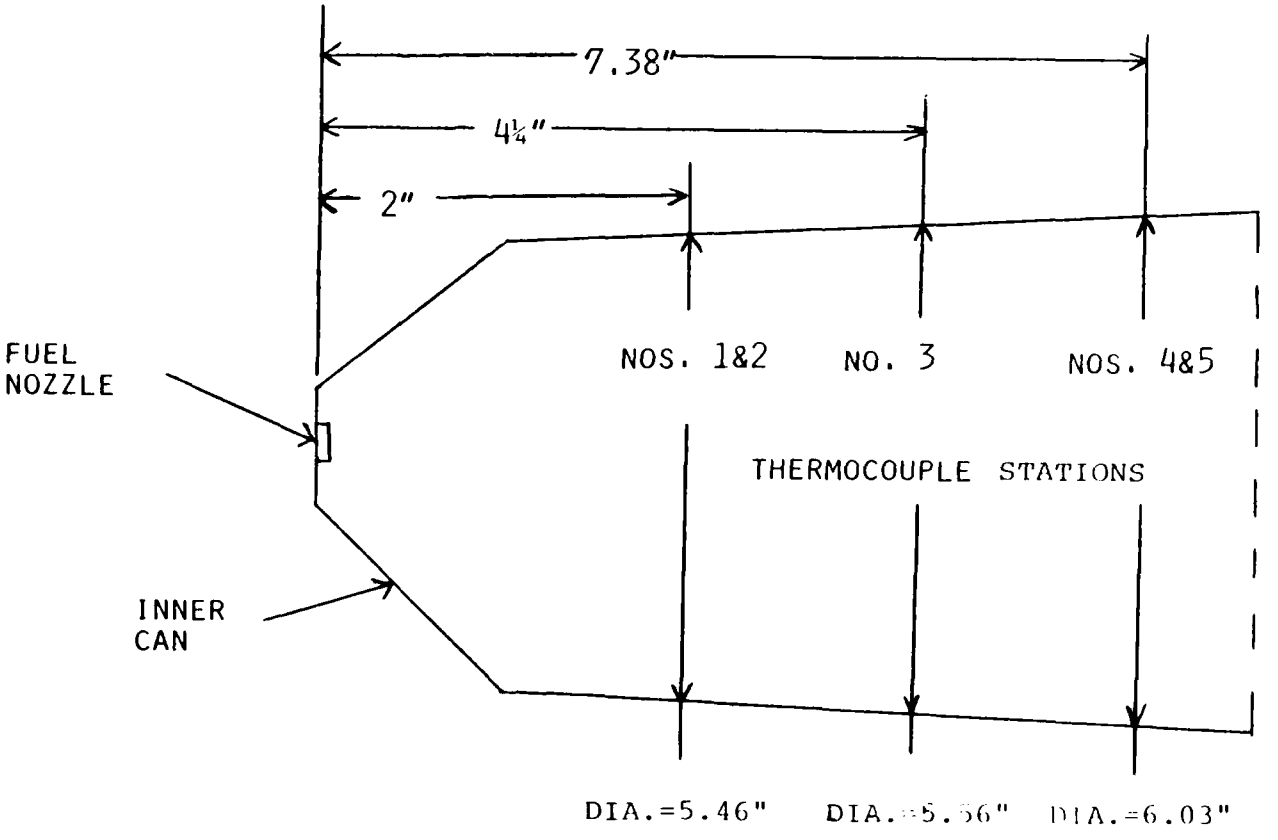

Figure 4. Combustor Thermocouple Placement (Side View)

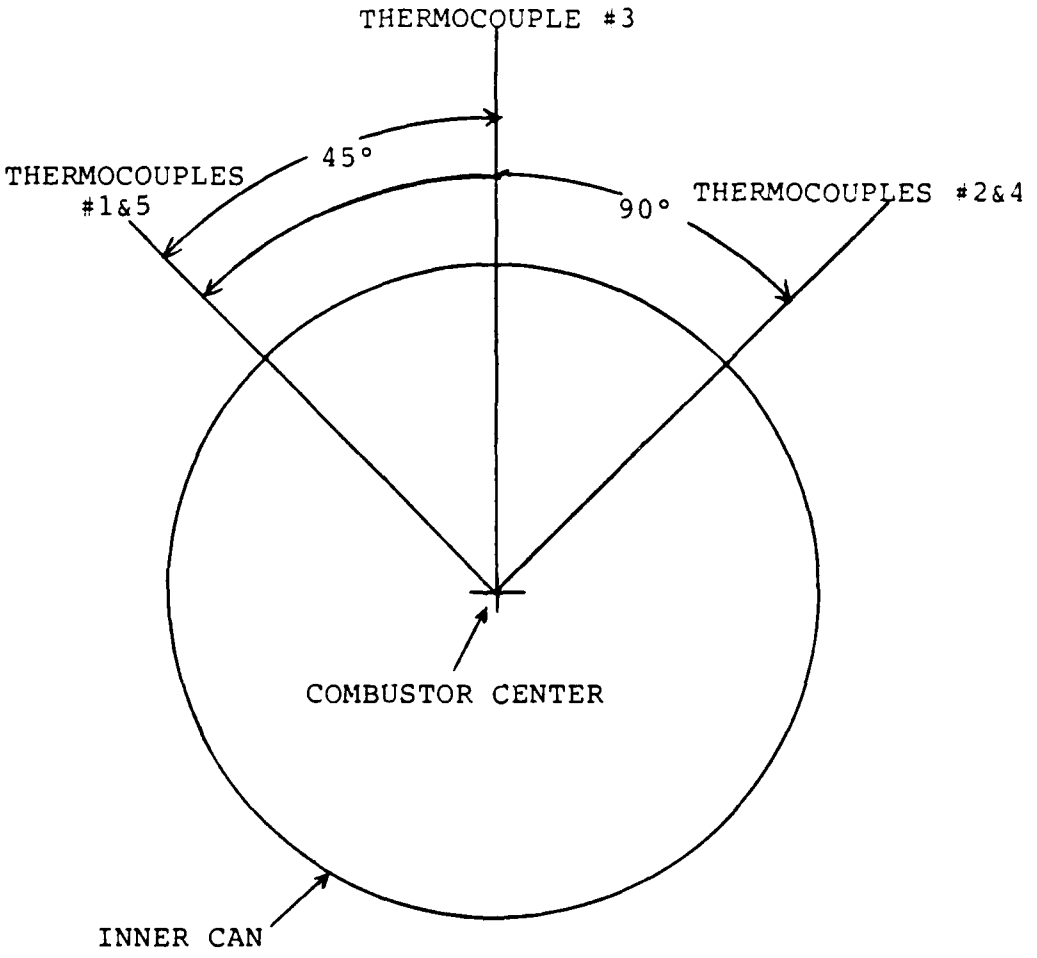

DISTANCE OF THERMOCOUPLES FROM COMBUSTOR CENTER

#1	2.23"
#2	1.73"
#3	2.28"
#4	2.01"
#5	NOT USED

Figure 5. Combustor Thermocouple Placement - End View

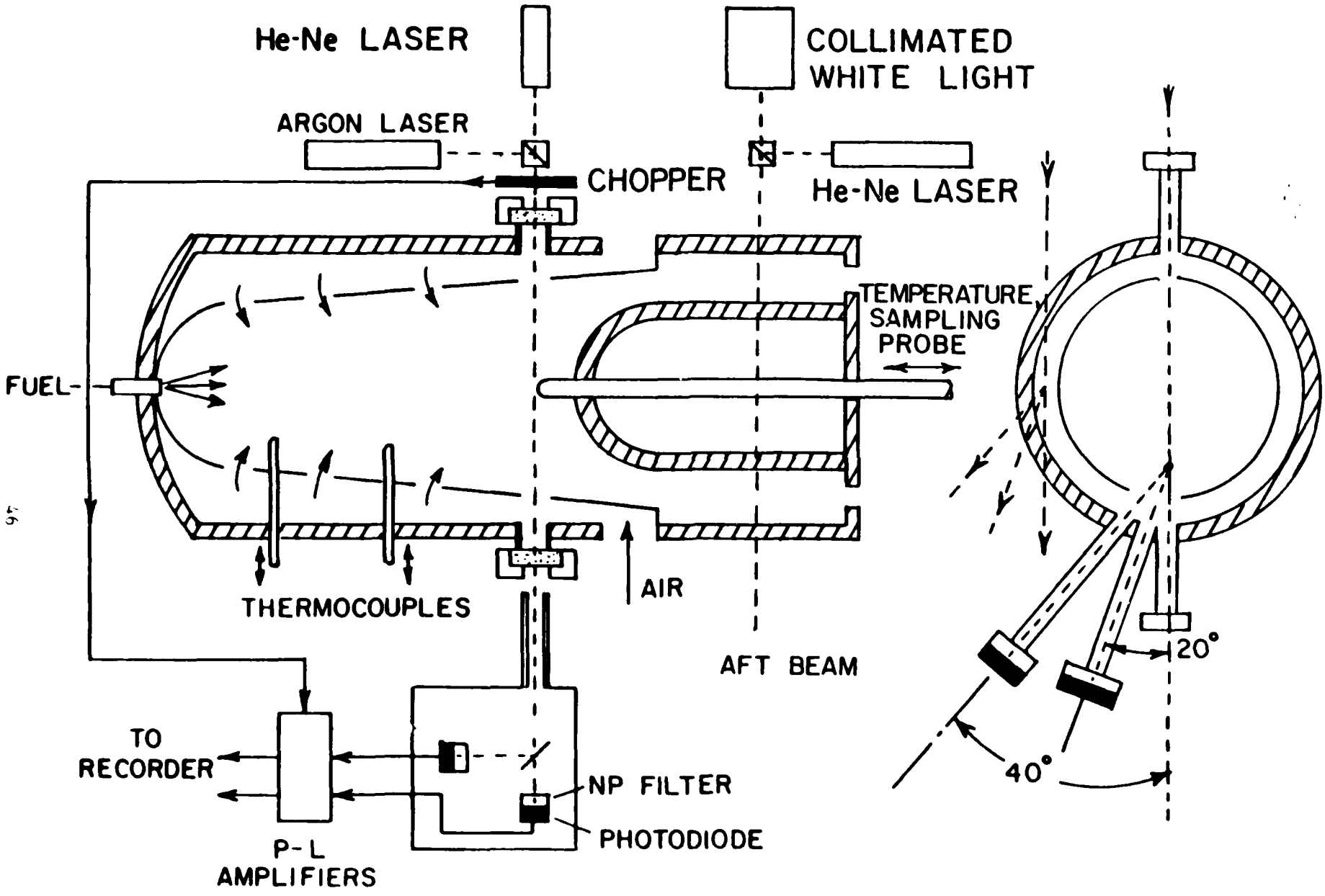

Figure 6. Schematic of T-63 Apparatus - Initial Configuration

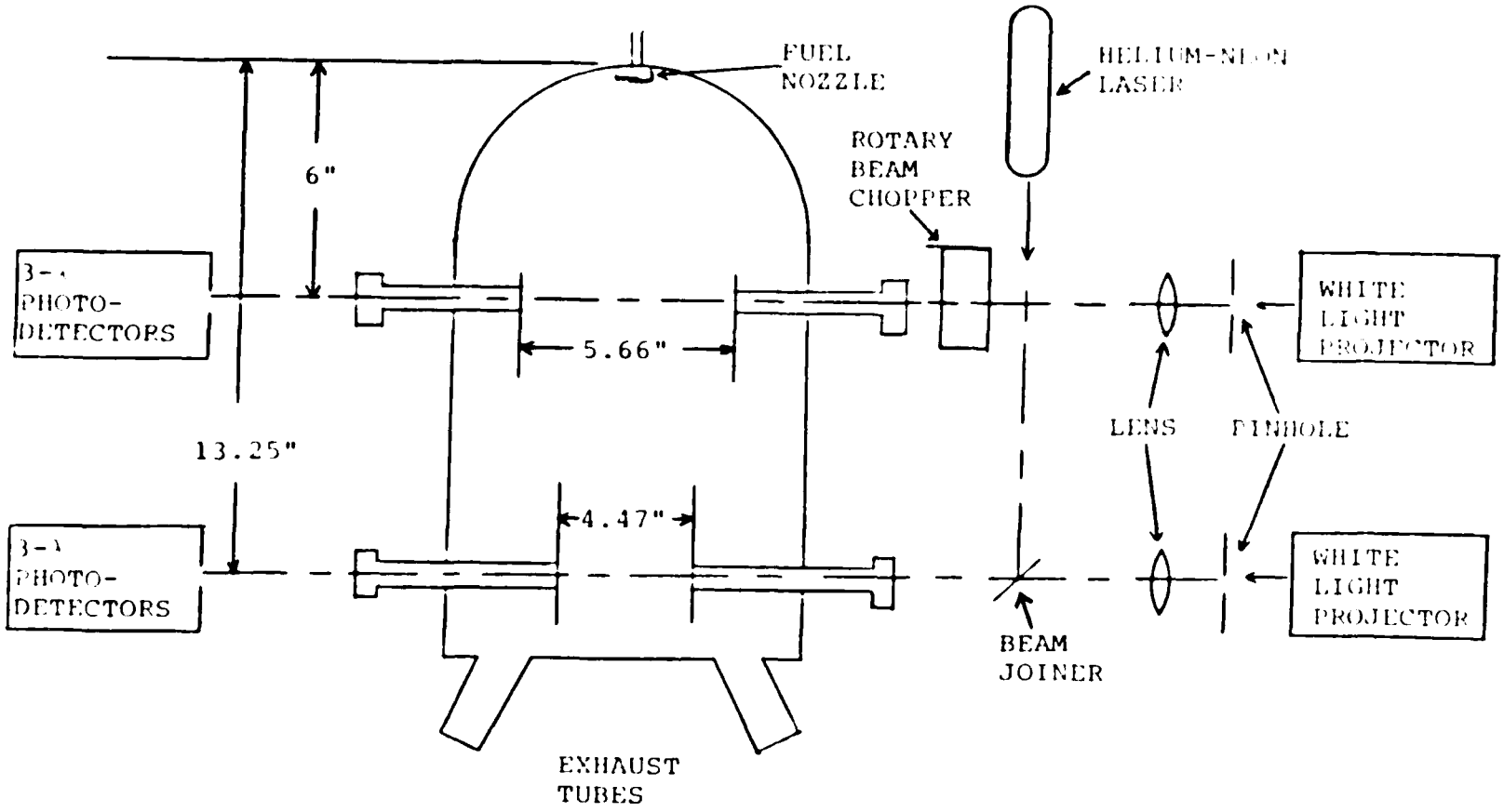

Figure 7. Schematic of Combustor Optical Measurement Paths (Top View)

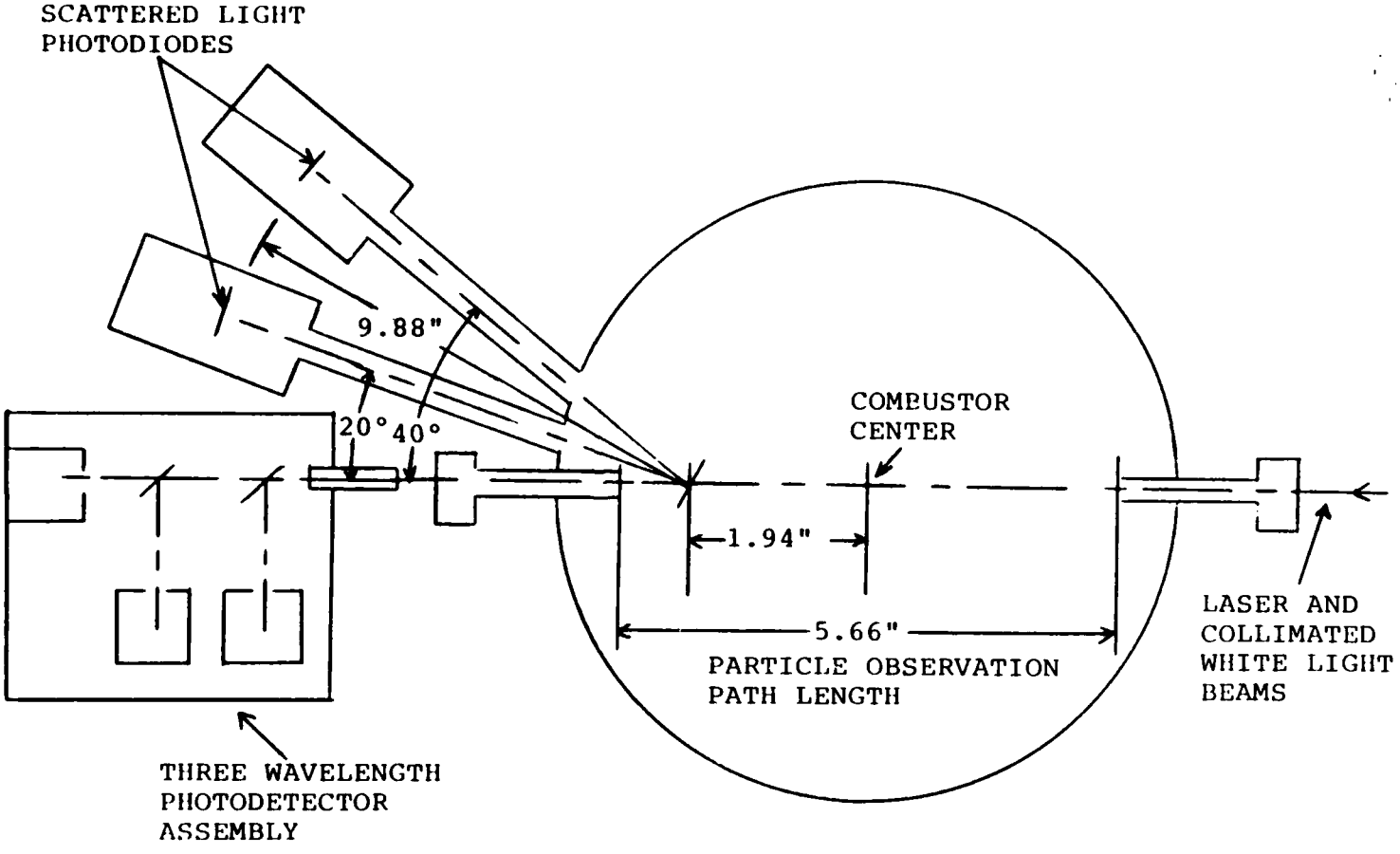

Figure 8. Schematic of Optical Path in Main Combustor Section (End View)

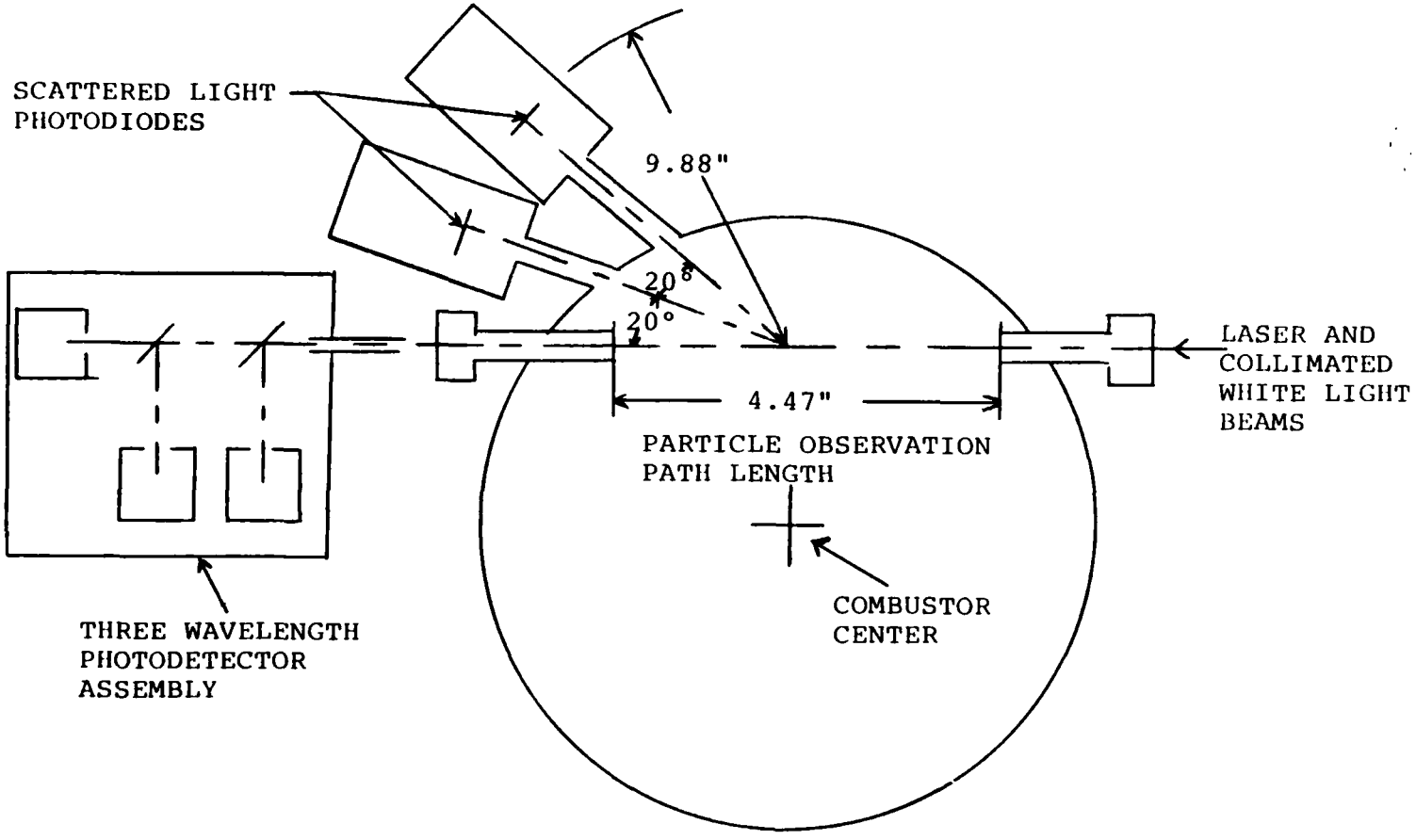

Figure 9. Schematic of Optical Path in Exhaust Section (End View)

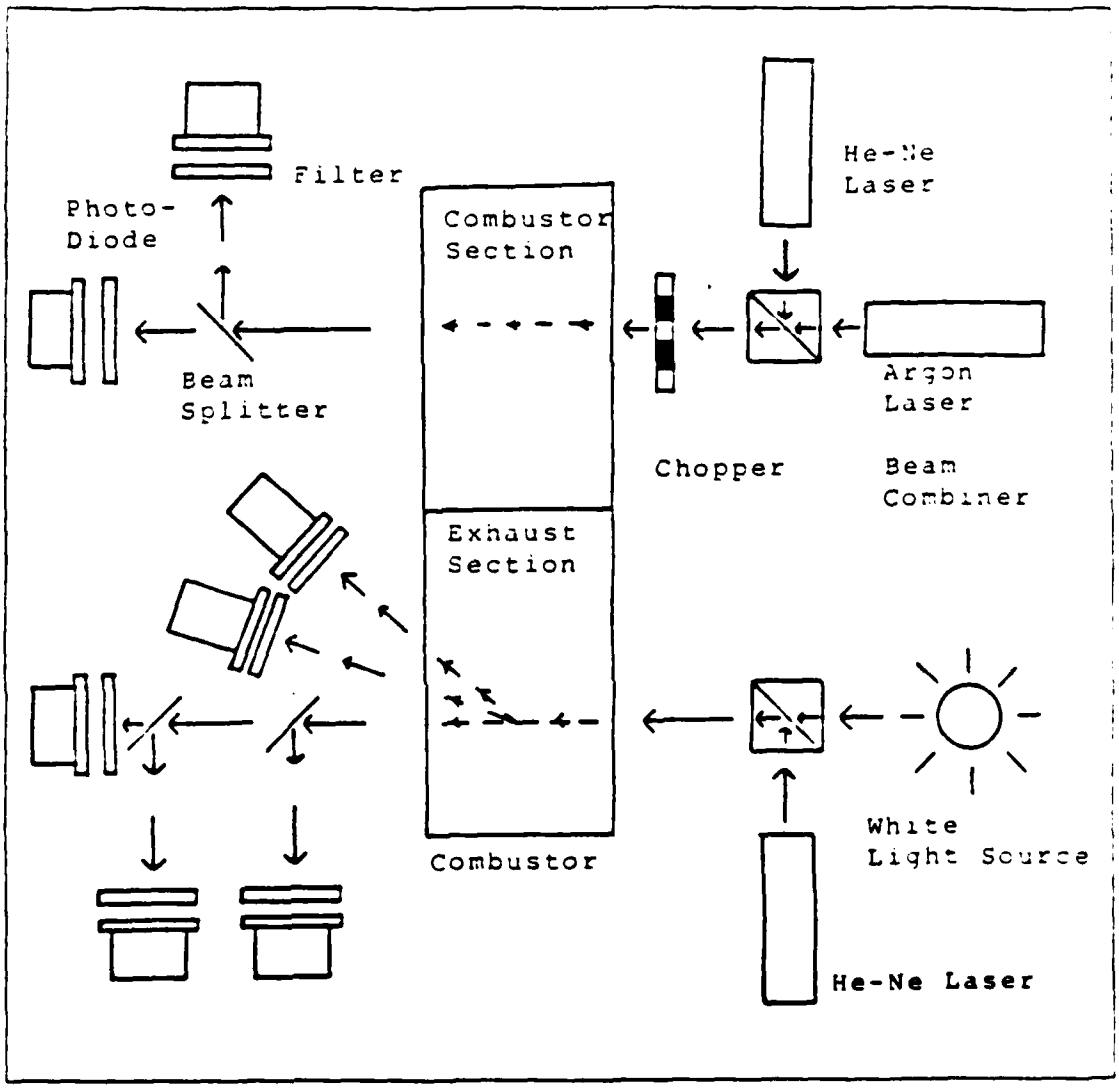

Figure 10. Setup of the Optical System to Measure Light Transmission and Scattering Intensities

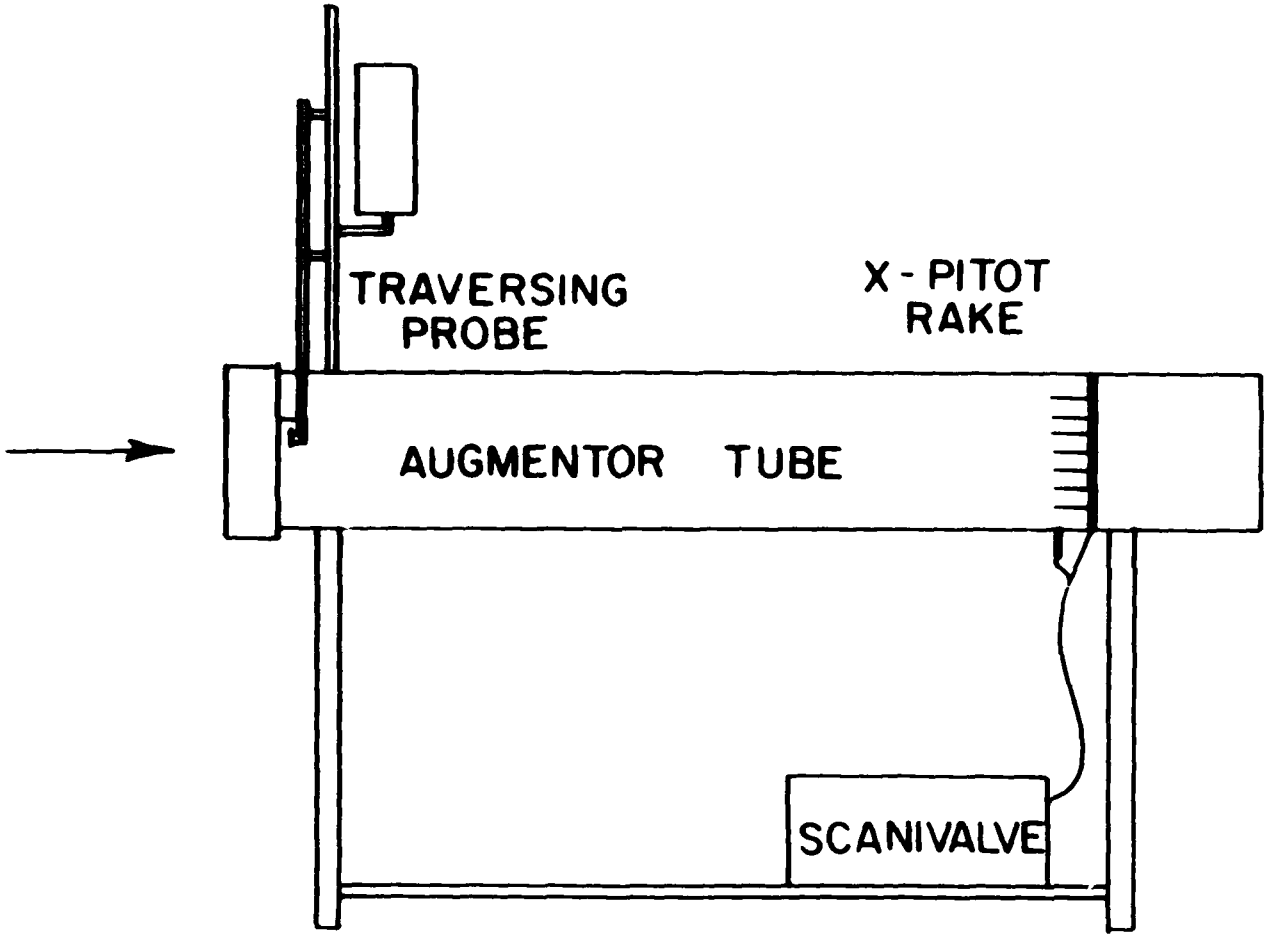

Figure 11. Schematic of Augmentor Tube

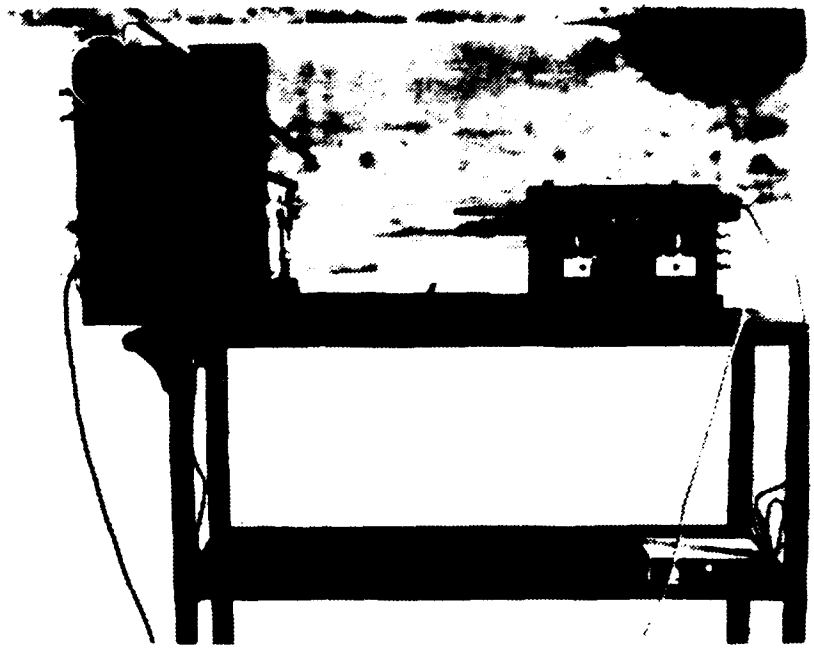

Figure 12. Photograph of Augmentor Tube Particle Sizing Apparatus

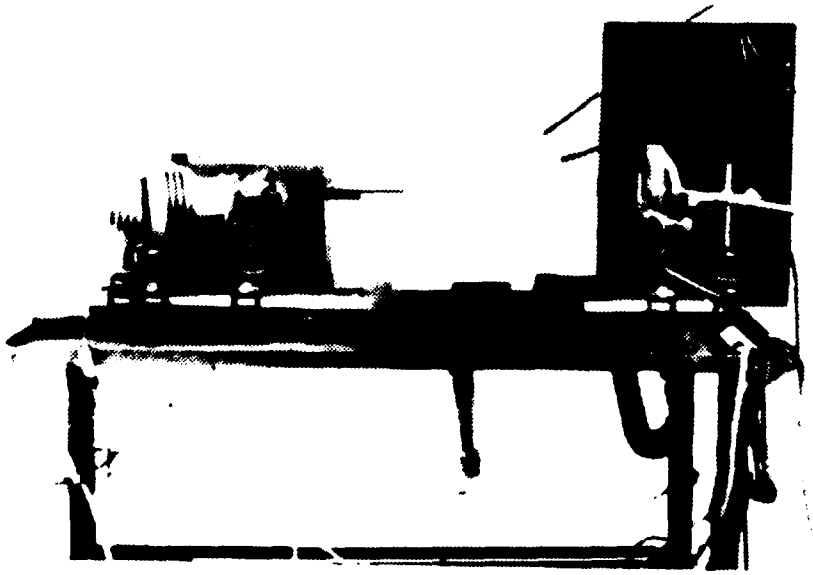

Figure 13. Photograph of Augmentor Tube Particle Sizing Apparatus

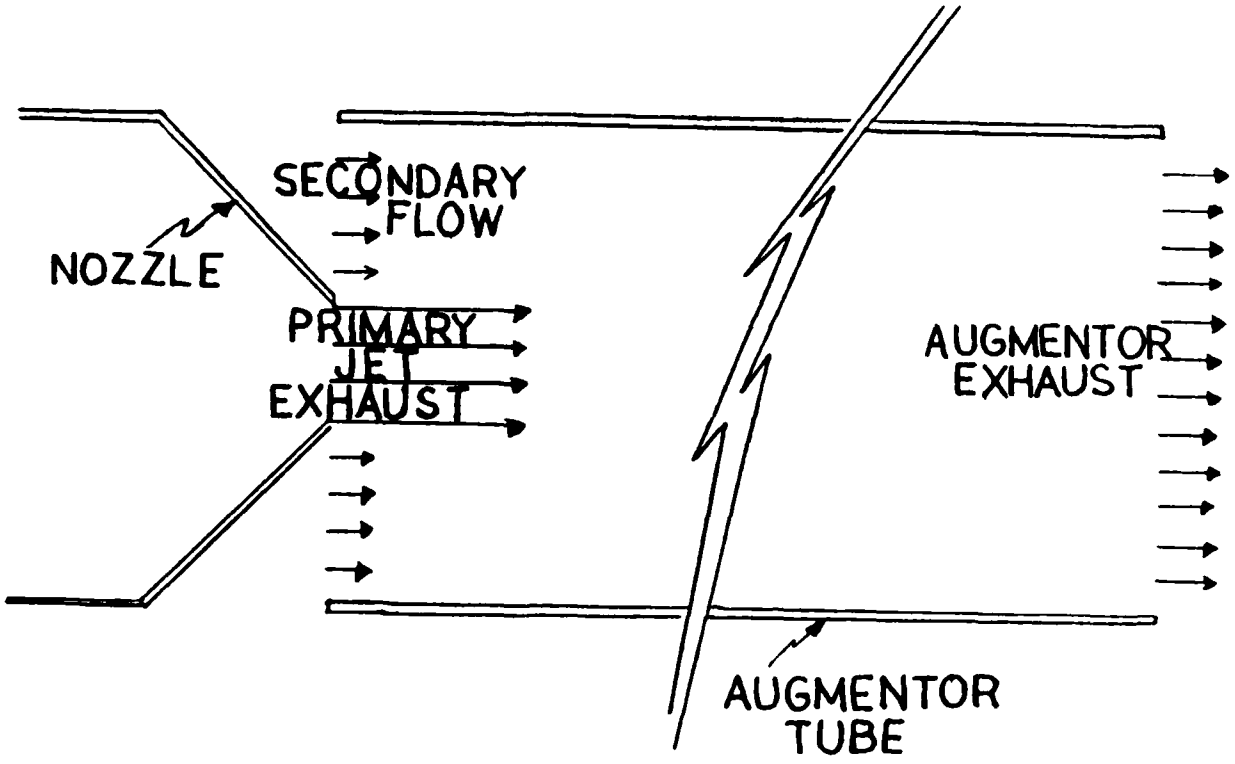

Figure 14. Augmentor Tube Flow Environment

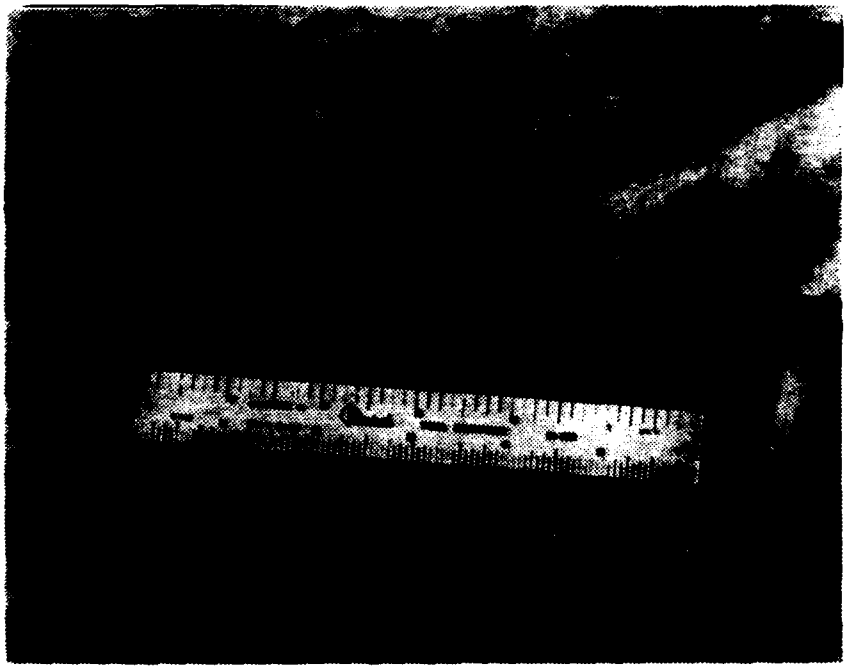

Figure 15. Traversing Kiel Probe

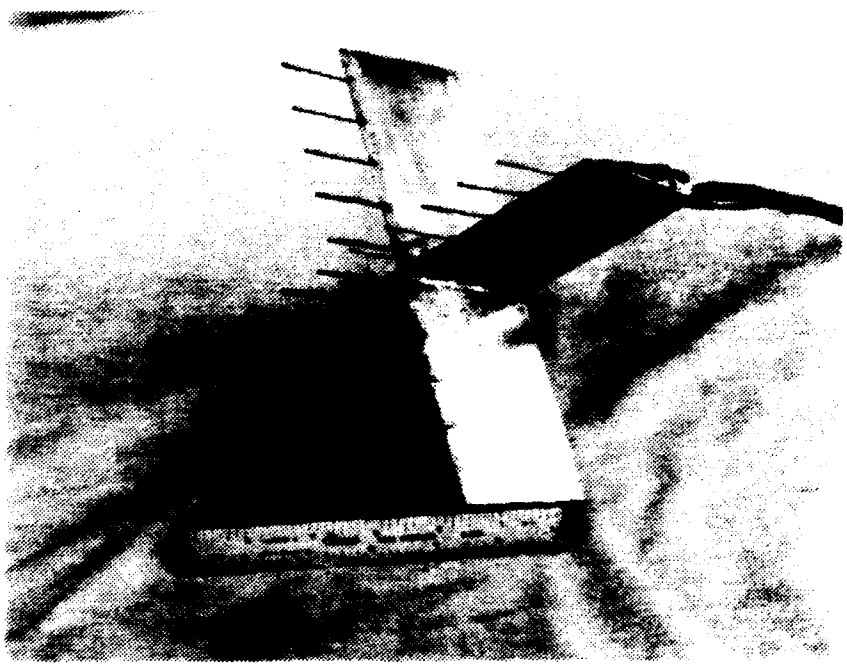

Figure 16. Stationary Pitot Rake

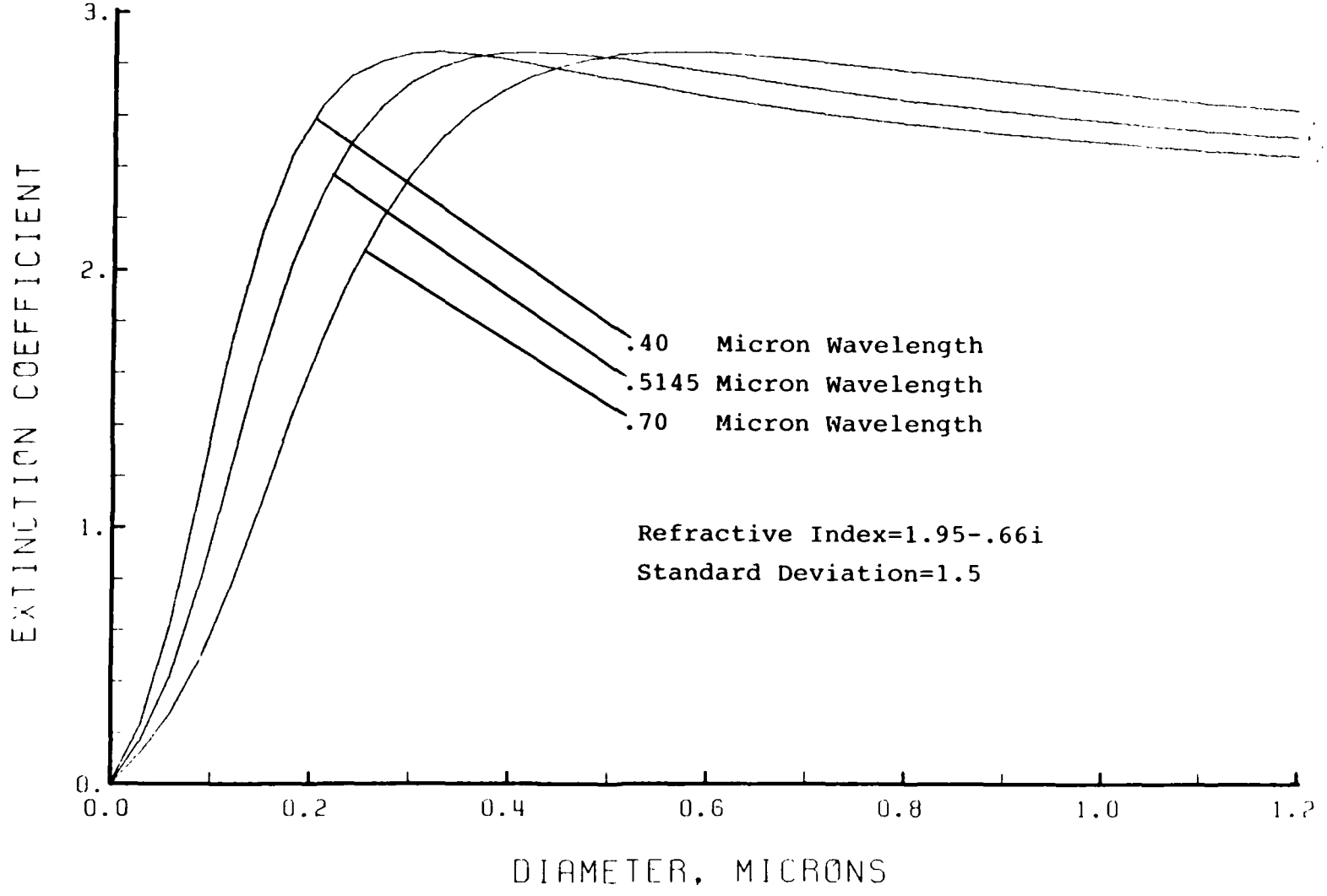

Figure 17. Extinction Coefficient vs. Particle size (D32)

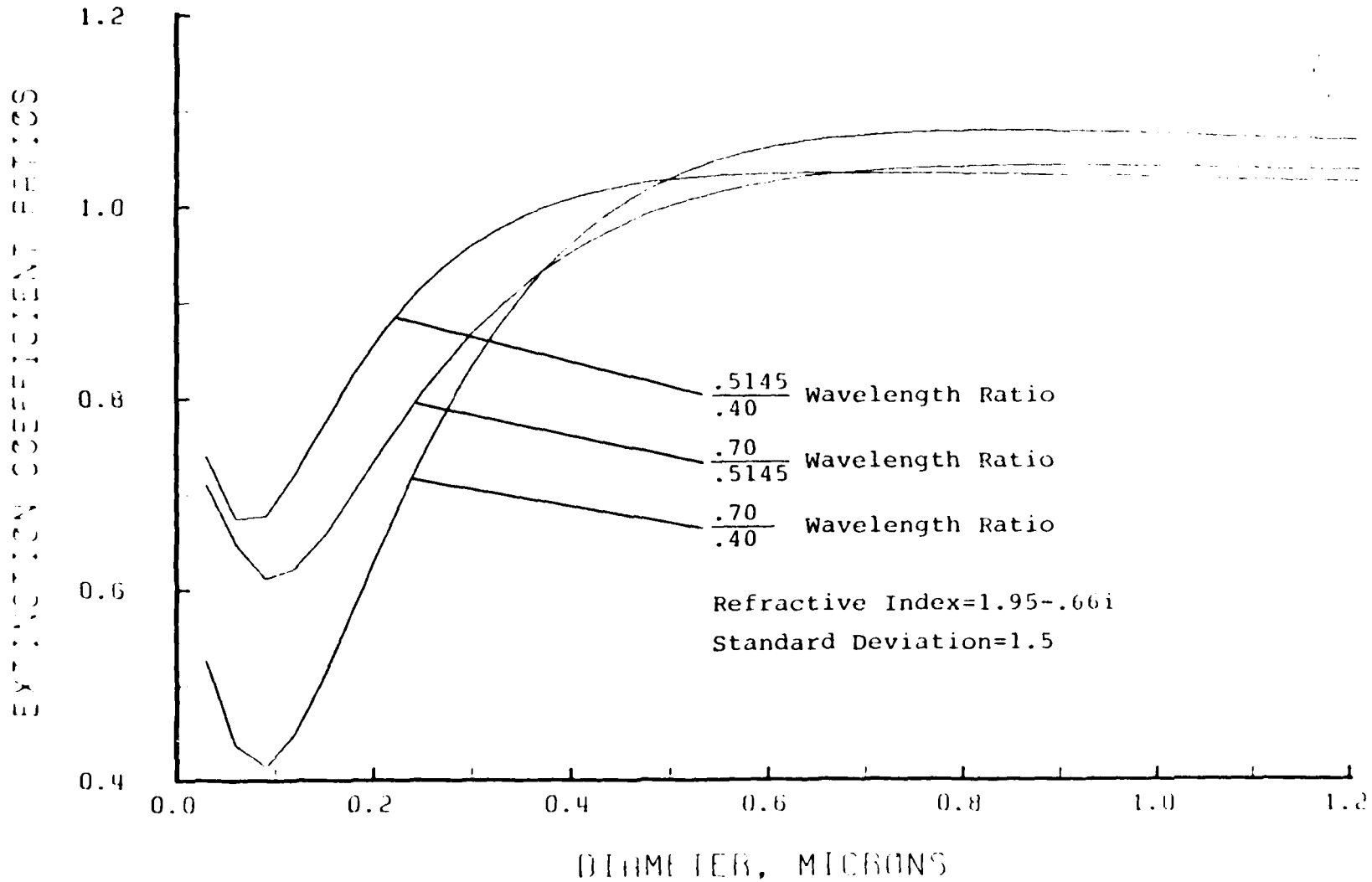

Figure 18. Extinction Coefficient Ratio vs. Particle Size (D32)

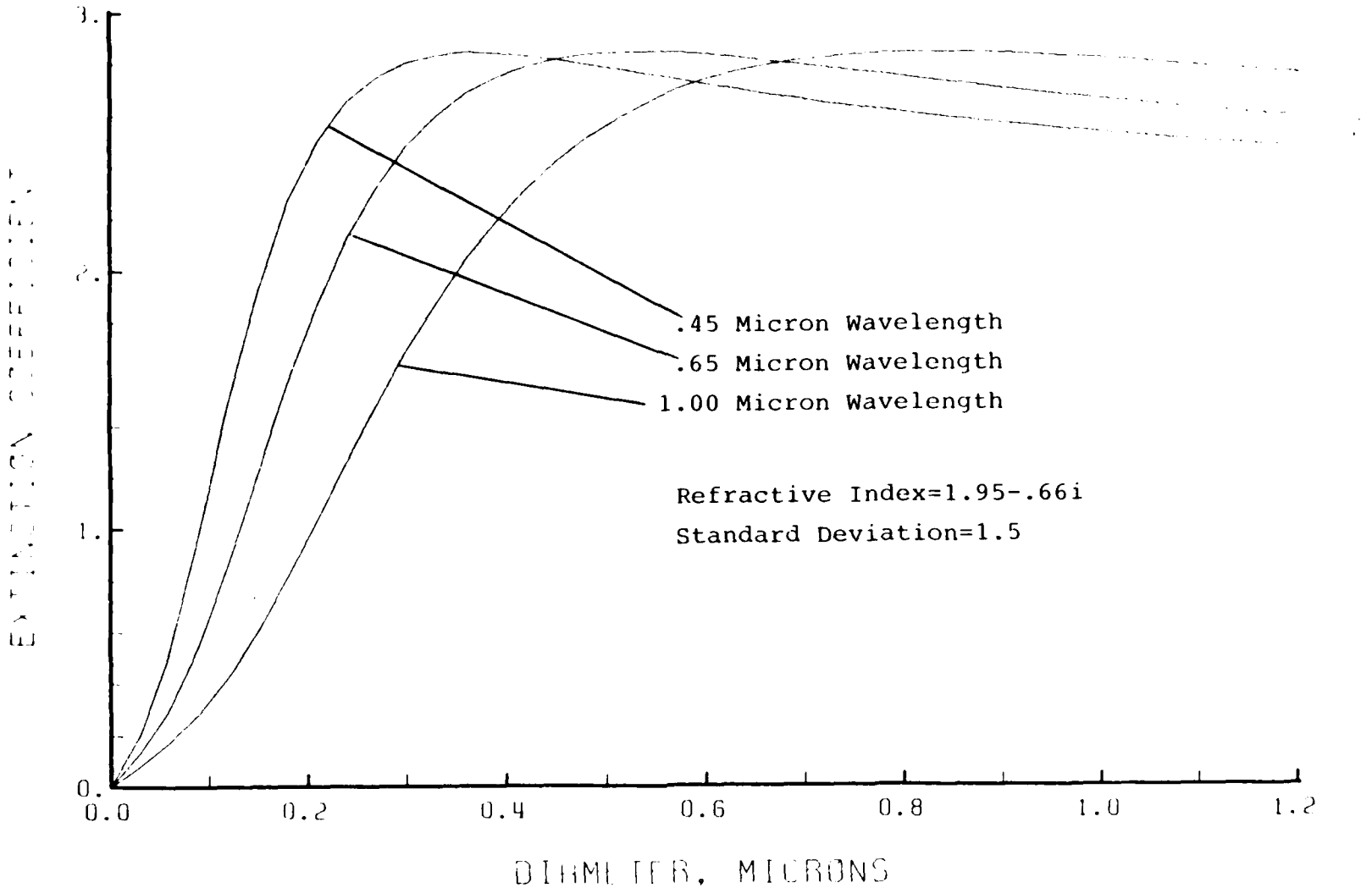

Figure 19. Extinction Coefficient vs. Particle Size (D32)

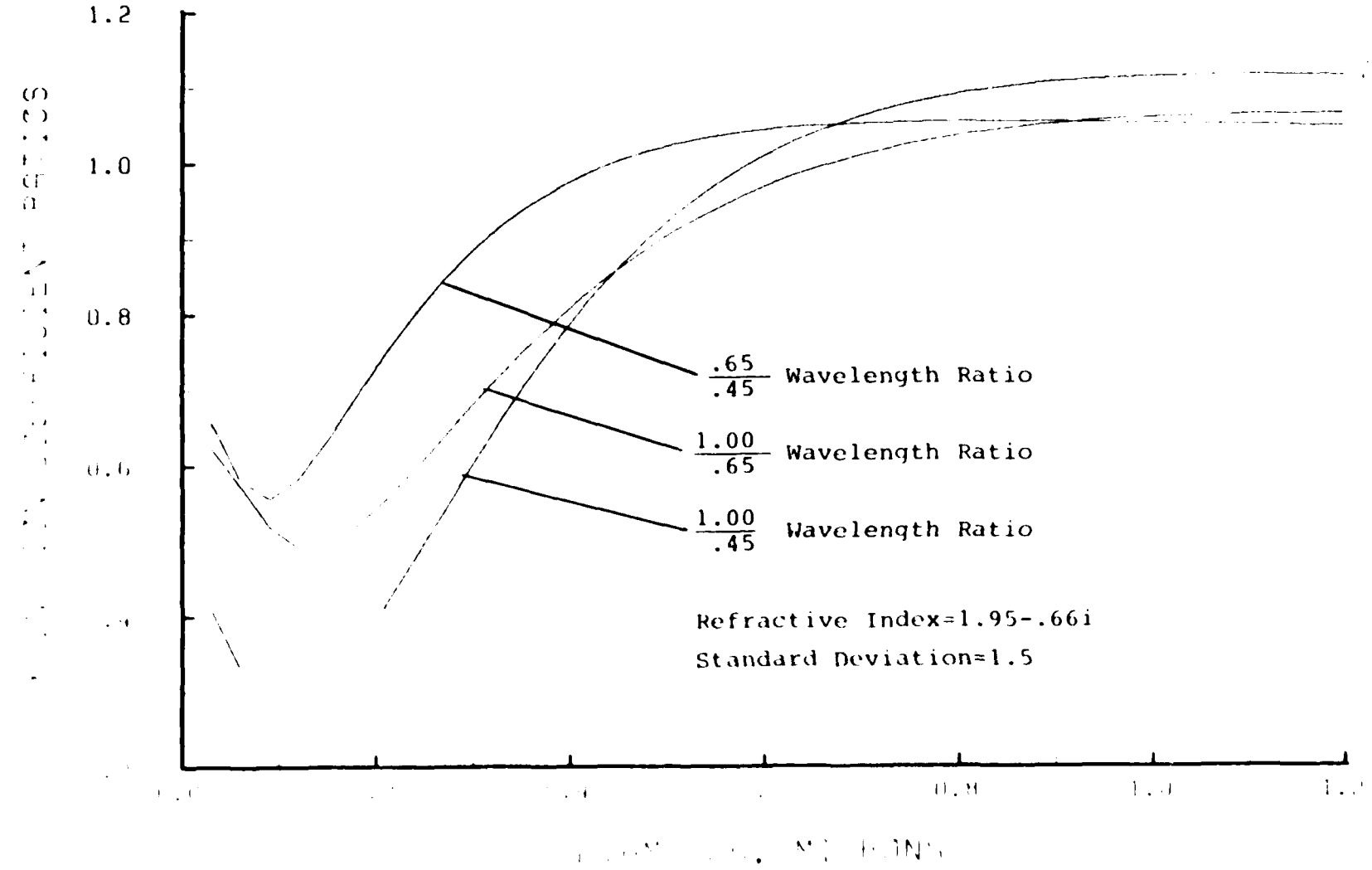

Figure 30. Extinction Coefficient Ratio vs. Particle Size (DIP)

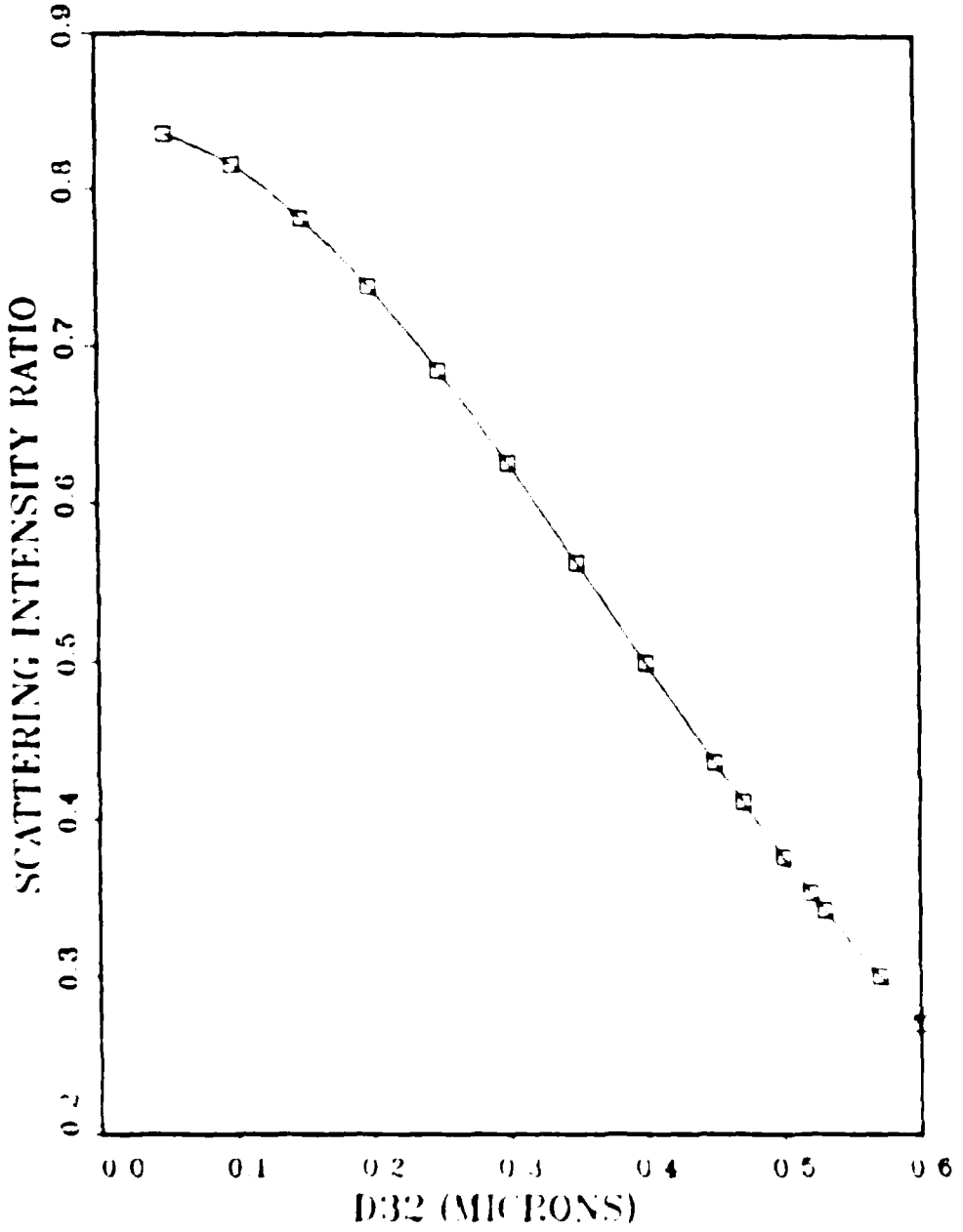

Figure 9 Scattered Light Intensity Ratio (45° 20°) vs. Particle Size (D32) for .6328 Micron Wavelength Light

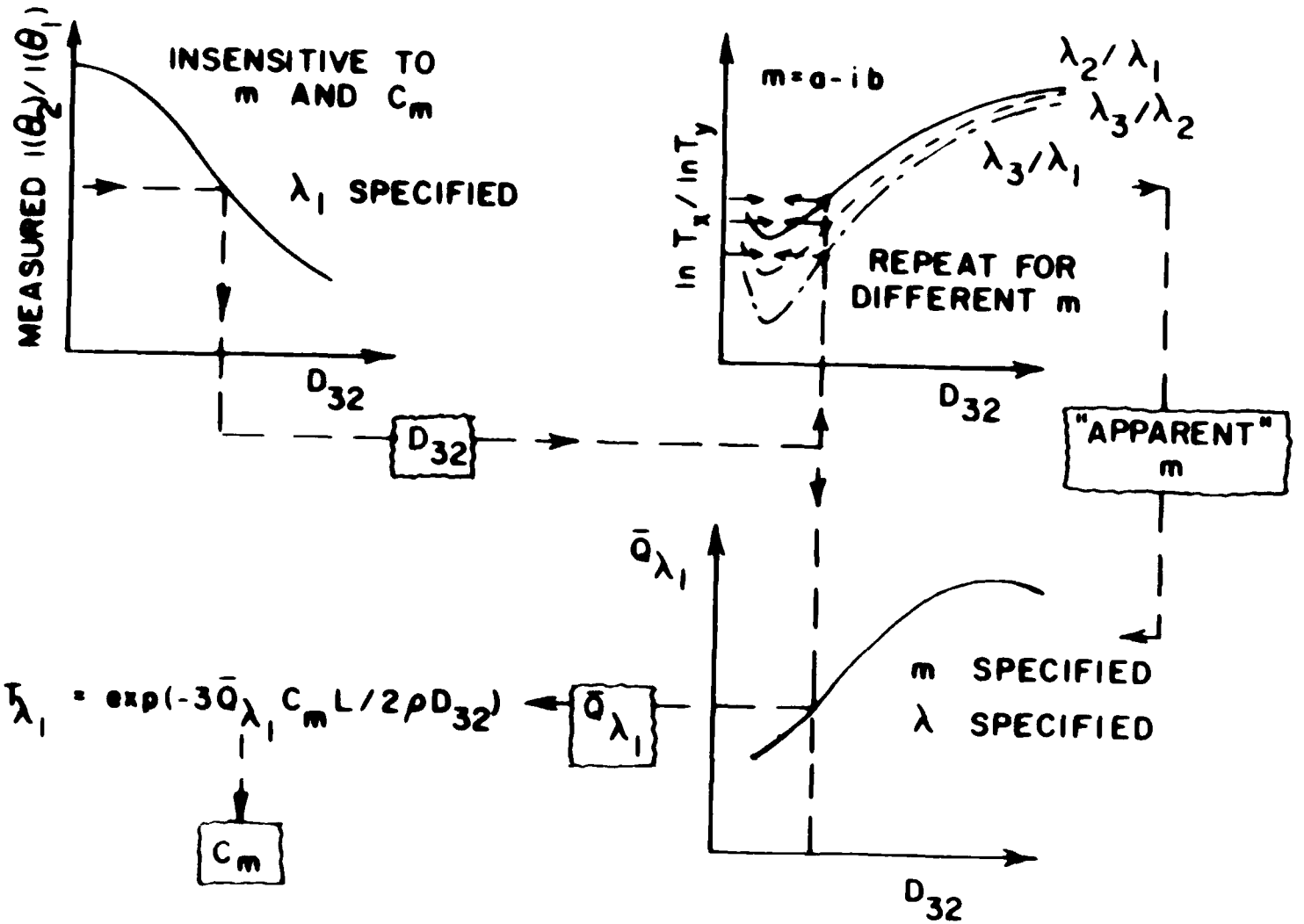
MEASURED $I(\theta_2)/I(\theta_1)$
INSENSITIVE TO m AND C_m
λ_1 SPECIFIED
D_{32}
D_{32}
$\ln T_x / \ln T_y$
m = a - ib
λ_2/λ_1
λ_3/λ_2
λ_3/λ_1
REPEAT FOR DIFFERENT m
D_{32}
"APPARENT" m
$\bar{Q}_{\lambda_1}$
m SPECIFIED
λ SPECIFIED
D_{32}
$T_{\lambda_1} = \exp(-3\bar{Q}_{\lambda_1} C_m L/2\rho D_{32})$
$\bar{Q}_{\lambda_1}$
C_m

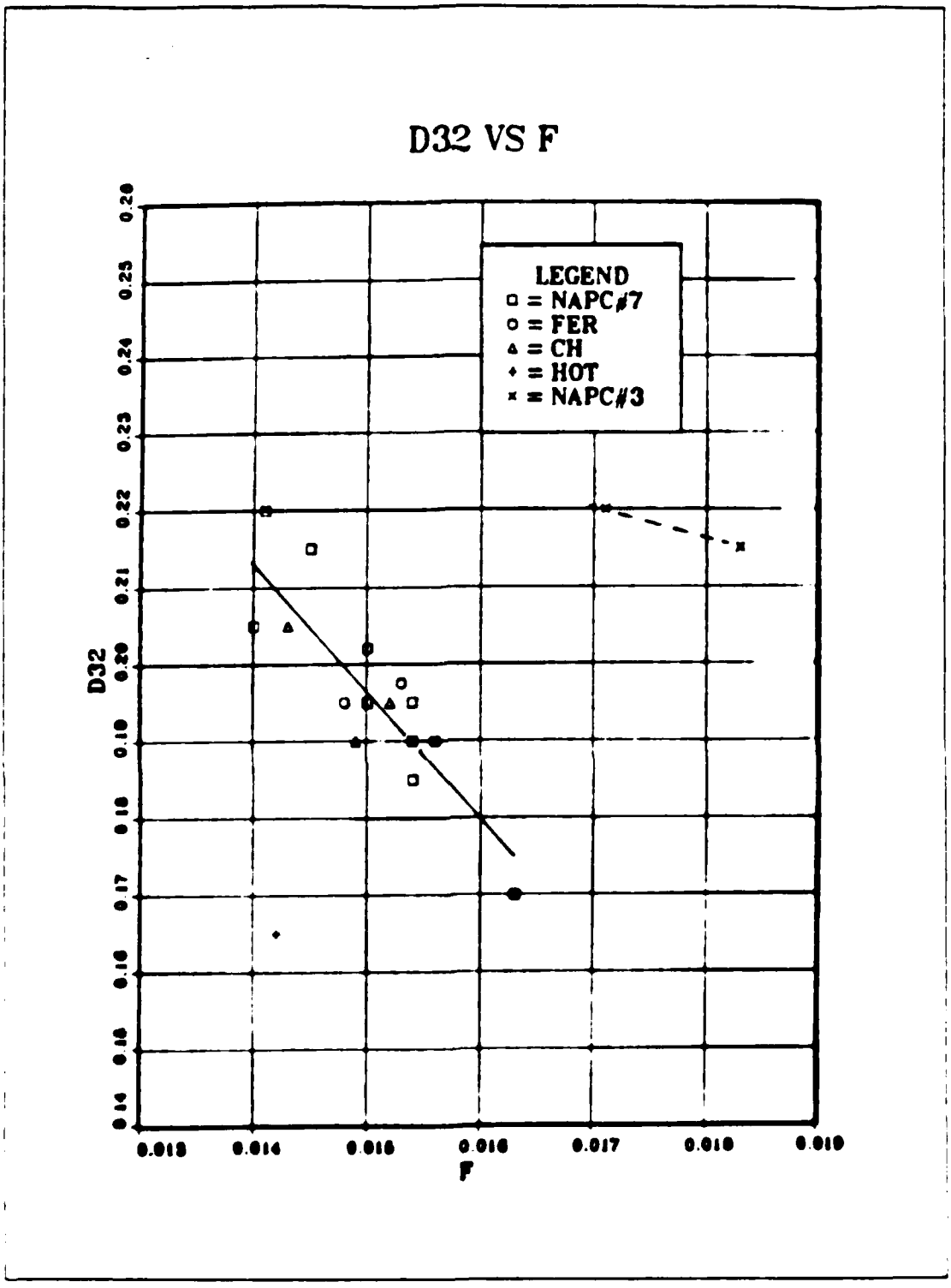

Figure 23. D32 vs Fuel-Air Ratio in Exhaust Region.

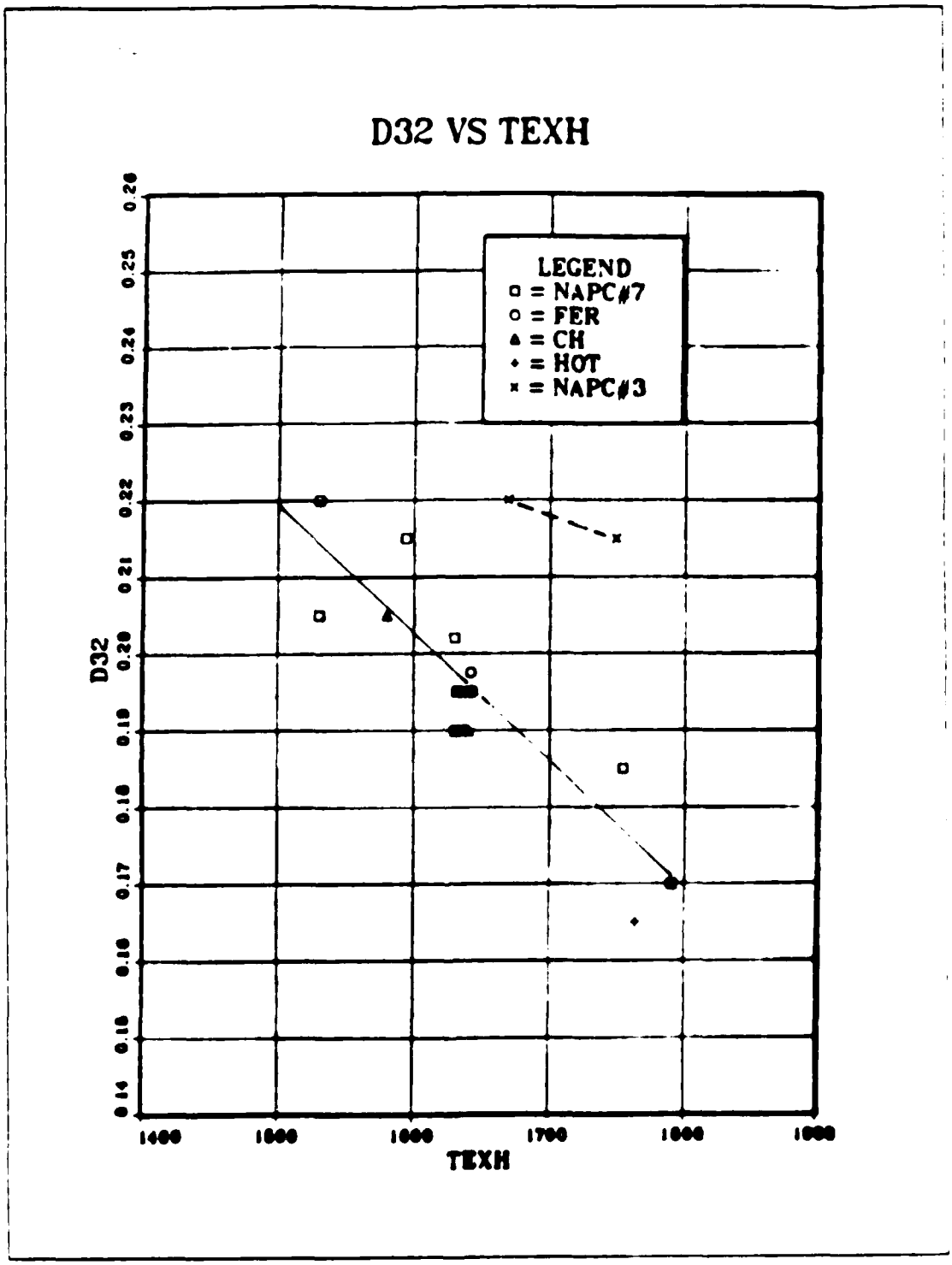

Figure 24. D32 vs Exhaust Temperature in Exhaust Region.

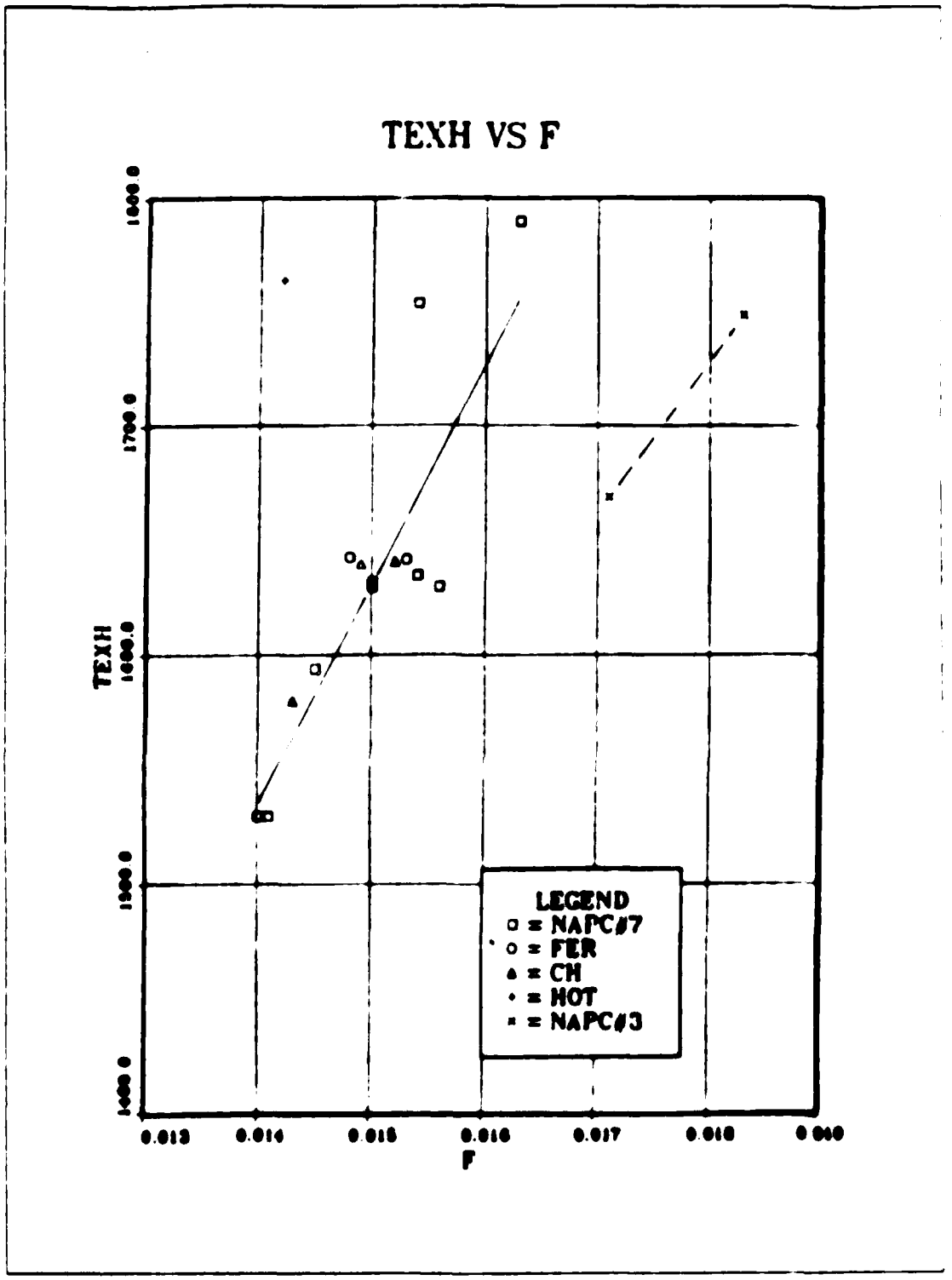

Figure 25. Exhaust Temperature vs Fuel-Air Ratio.

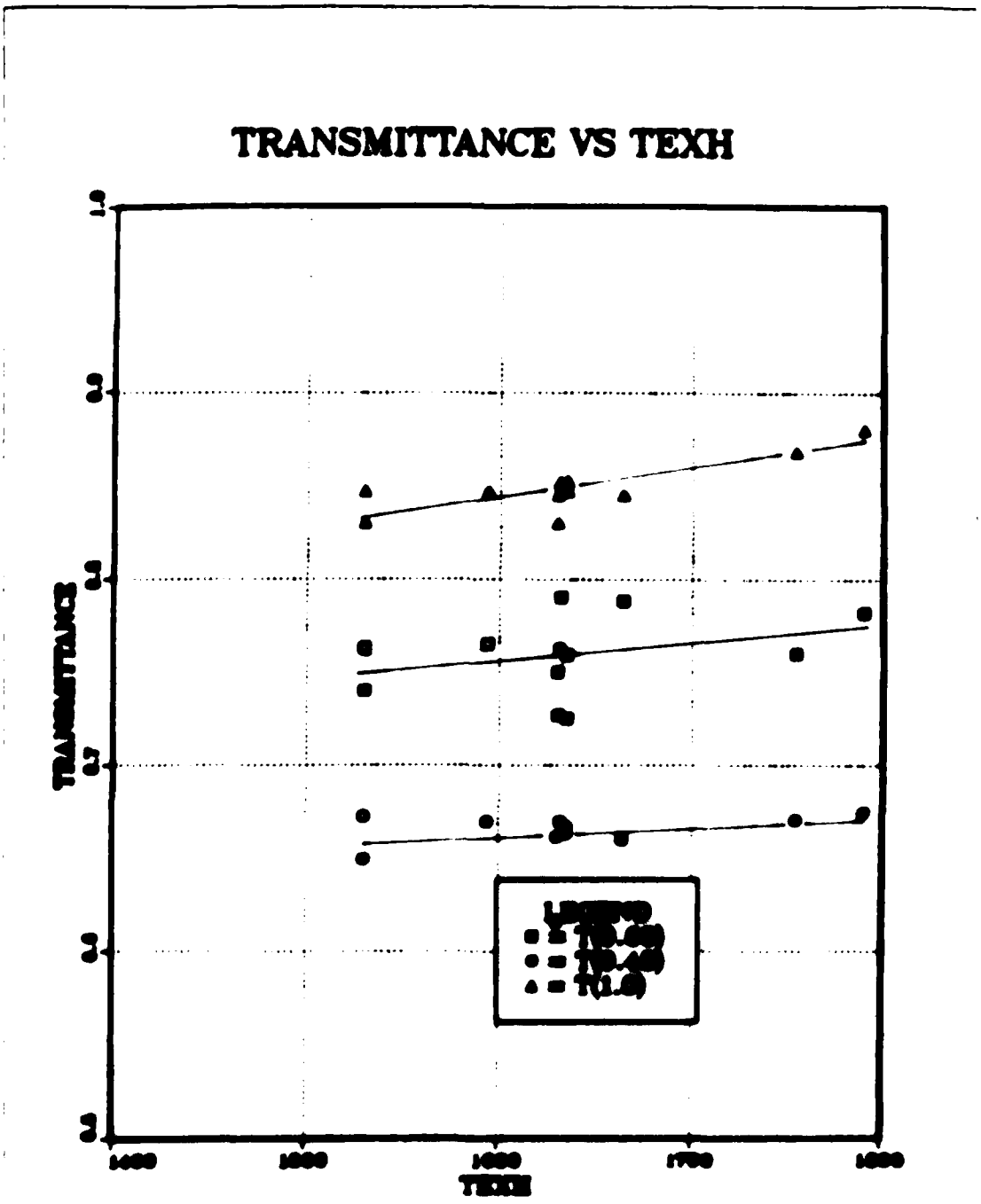

Figure [illegible] Transmittance vs Exhaust Temperature [illegible] Exhaust Region.

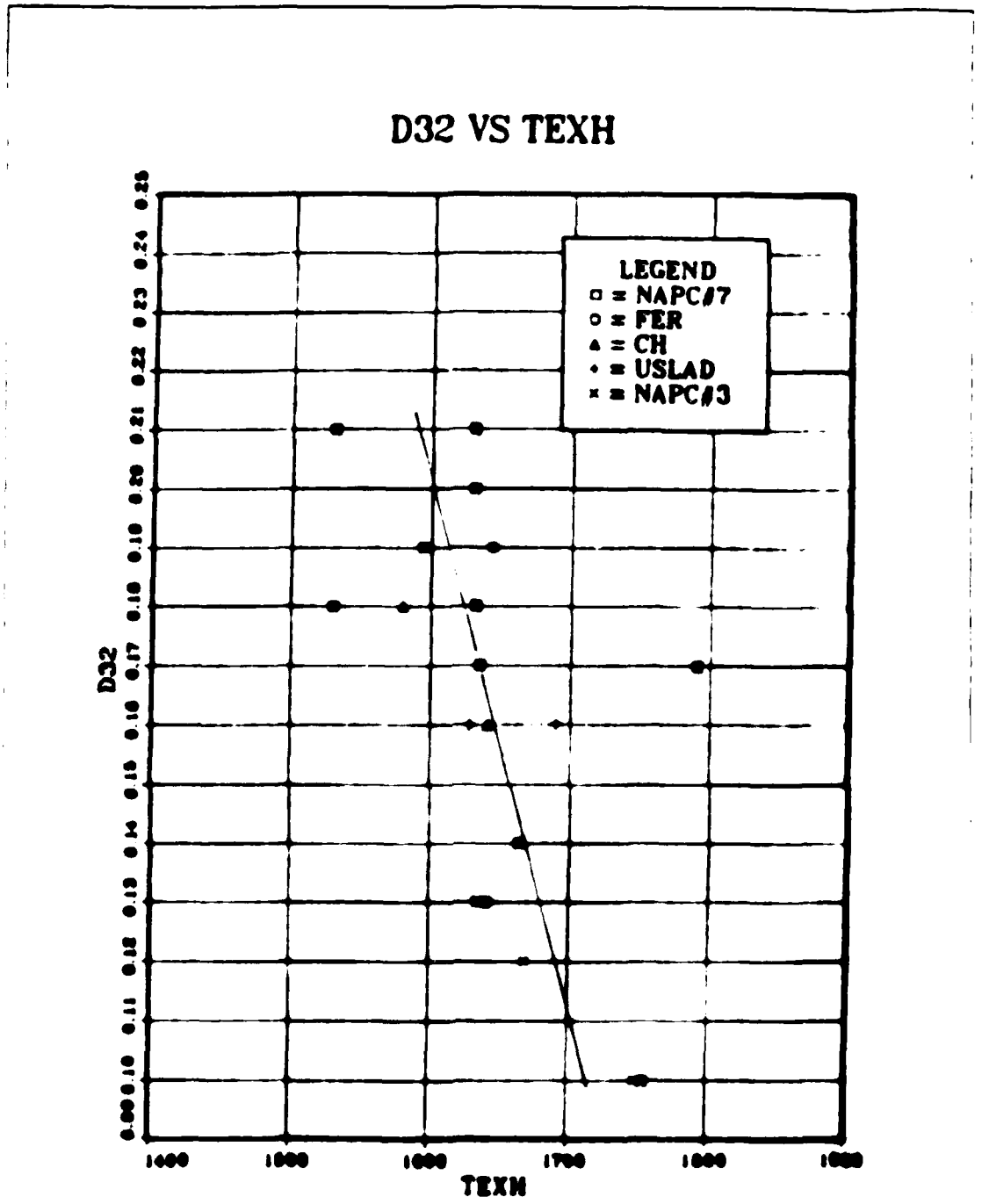

Figure . D32 vs Exhaust Temperature in Combustor Region.

VELOCITY PROFILES

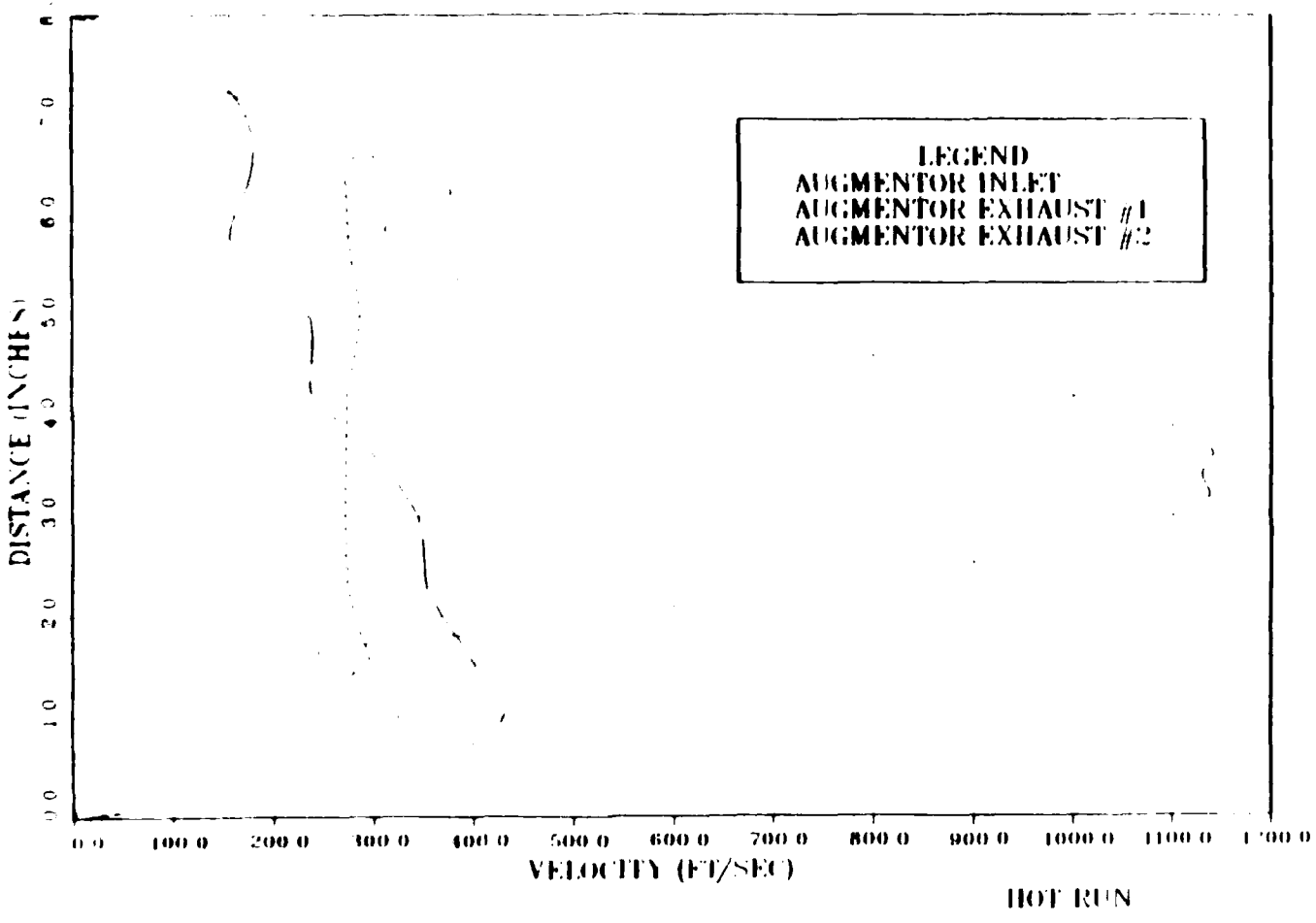

Figure 28. Augmentor Tube Velocity Profiles, S = 12 in., AR = 3.8

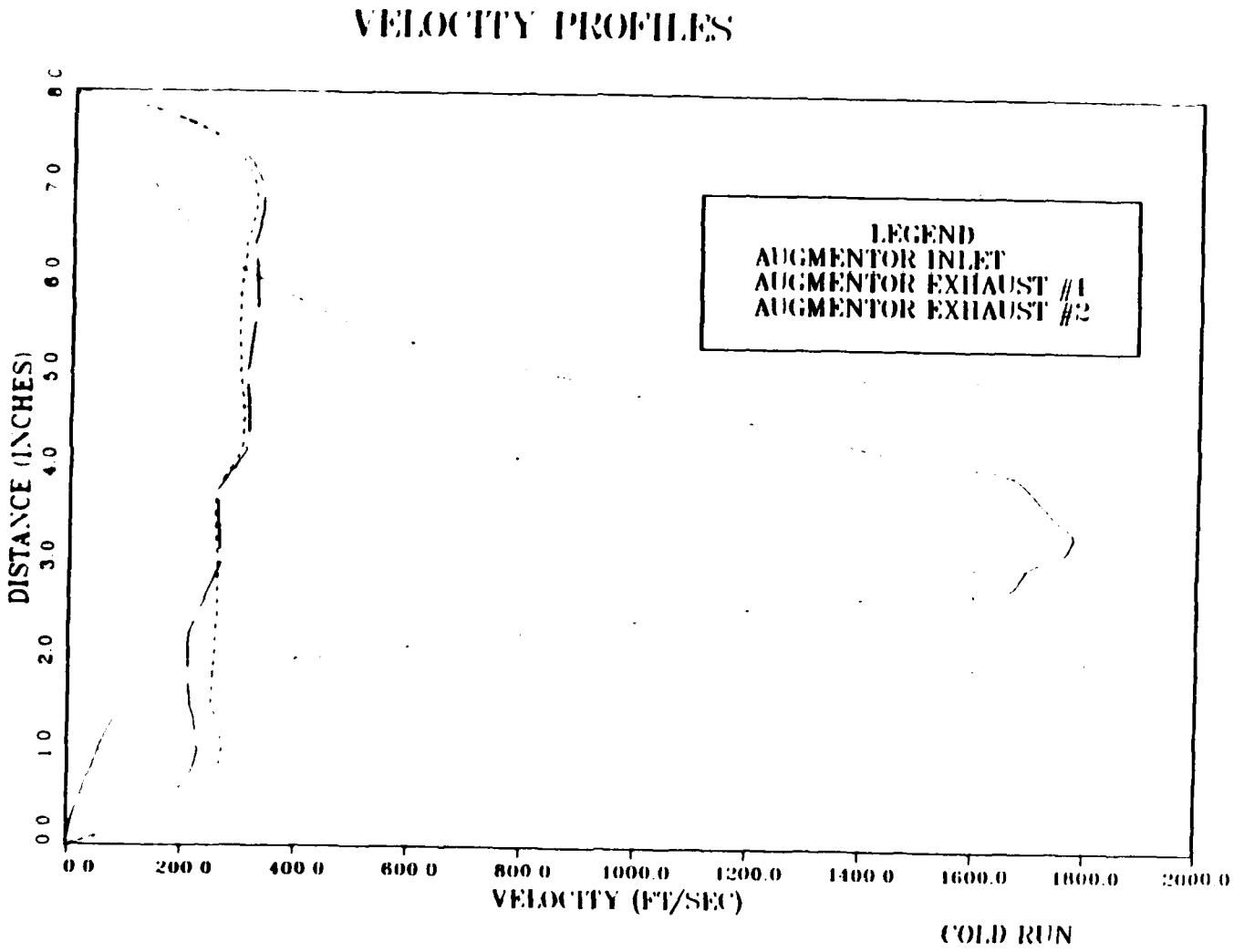

Figure 29. Augmentor Tube Velocity Profiles, S = 3 in., AR = 5.2

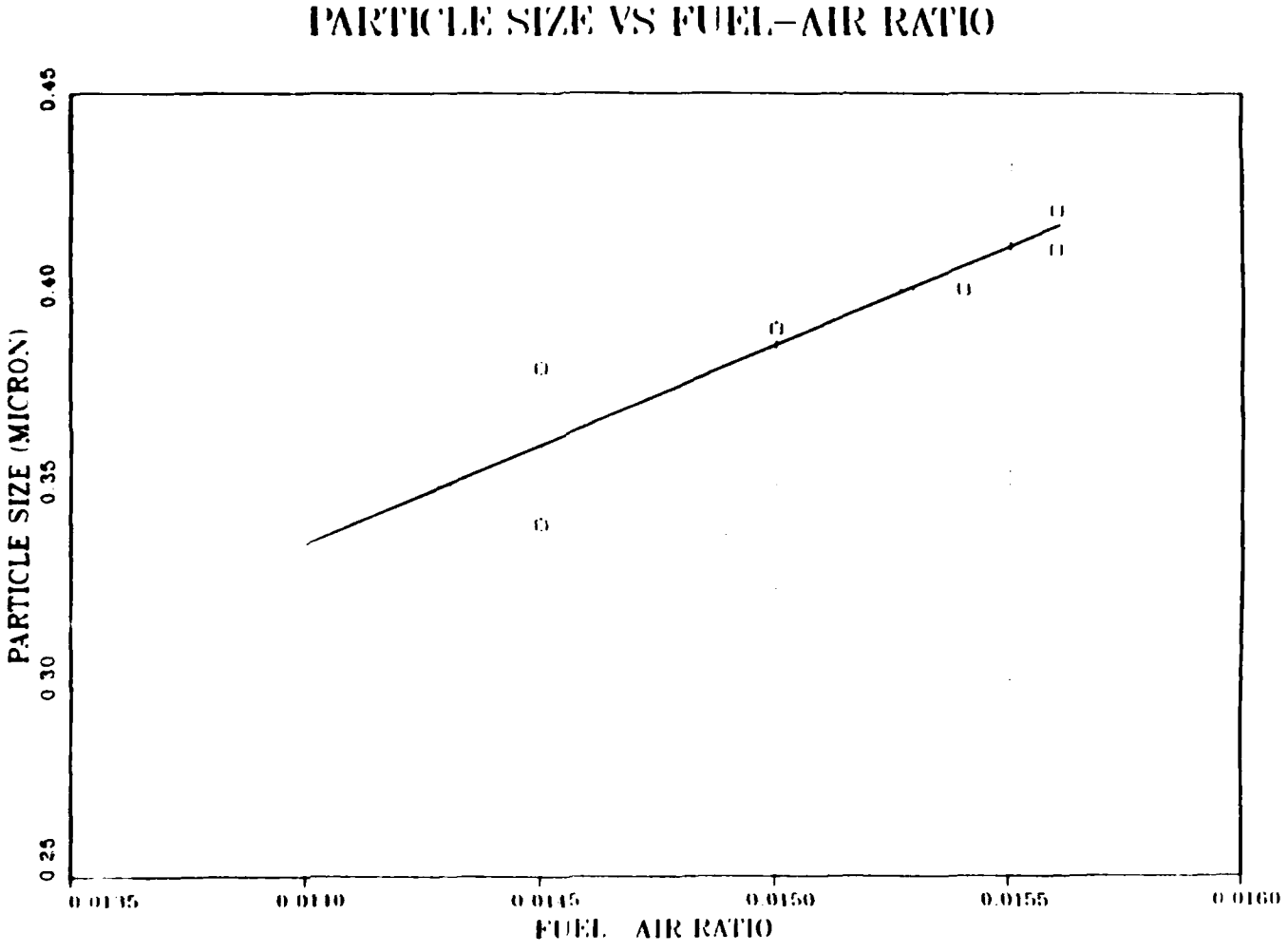

Figure 30. D32 vs. Fuel-Air Ratio at Augmentor Tube Exhaust

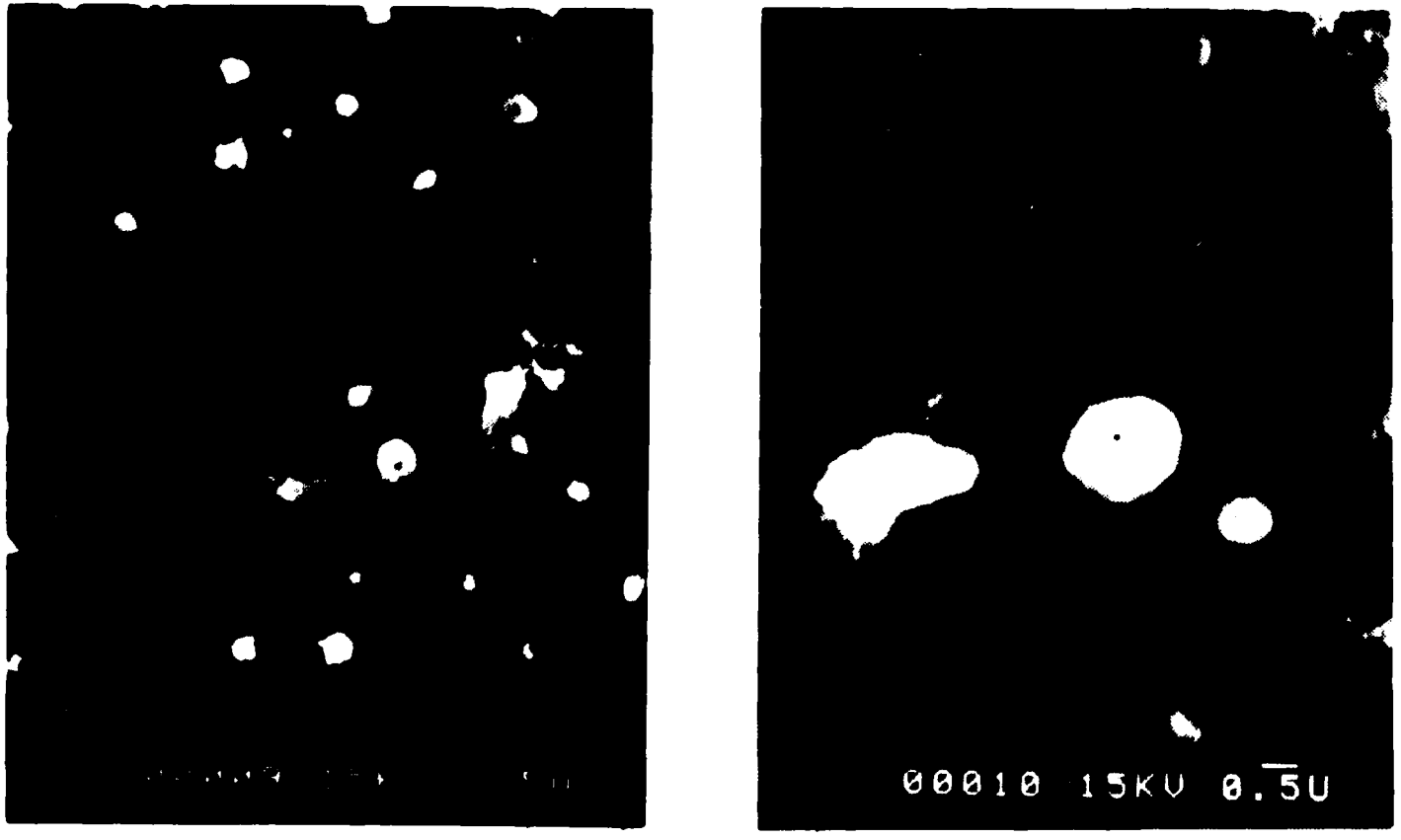

Figure 41. Scanning Electron Microscope Photograph, Impact Sample

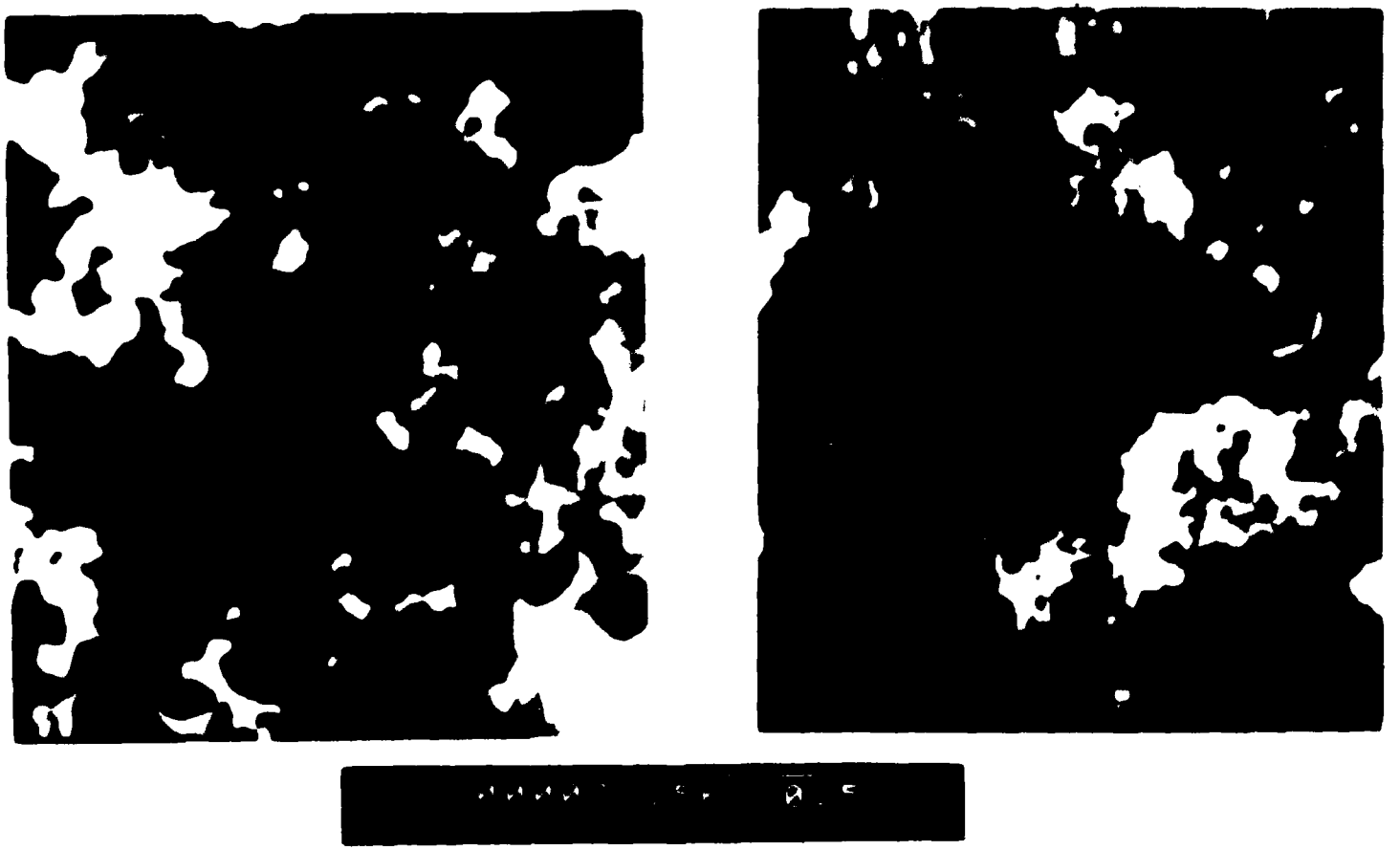

LIST OF REFERENCES

1. Naval Postgraduate school report No. NPS67-85-004, An Investigation of the Effects of Fuel Composition on Combustion Characteristics in a T-63 Combustor, by R.W. Dubeau, et. al., March 1985.

2. Naval Postgraduate School Report No. NPS67-80-014, Validation of a Two-dimensional Primitive Variable Computer Code for Flow Field in Jet Engine Test Cells, by P.J. Mallon, P.J. Hickey, D.W. Netzer, October 1980.

3. Naval Postgraduate School Report No. NPS67-81-001, Temperature Dependence of Gas Properties in Polynomial Form, by J.R. Andrews, O. Biblarz, January 1981.

4. Cashdollar, K.L., Lee, C.K., and Singer, J.M., "Three-Wavelength Light Transmission Technique to Measure Smoke Particle Size and Concentration," Applied Optics, Volume 18, Number 11, June 1979.

5. R.A. Dobbins & G.S. Jizmagian, "Particle Size Measurements Based on Use of Mean Scattering Cross-Sections," J. Opt. Soc. of Am, Vol 56, No. 10, Oct. 1966, pp. 1351-1354.

6. J.R. Hodkinson, "Particle Sizing by Means of the Forward Scattering Lobe," Applied Optics, Vol. 5, No. 5, May 1966, pp. 839-844.

7. S. Boron & B. Waldie, "Particle Sizing by Forward Lobe Scattered Intensity-Ratio Technique: Errors Introduced by Applying Diffraction Theory in the Mie Regime," Applied Optics, Vol. 17, No. 10, May 1978, pp. 1644-1648.

8. R.A. Dobbins, L. Grocco & I. Glassman, "Measurement of Mean Particle Sizes of Sprays from Diffractively Scattered Light," AIAA J., Vol. I, No. 8, Aug. 1963, pp. 1882-1886.

9. R.A. Powell et. al., "Combustion Generated Smoke Diagnostics by Means of Optical Techniques," AIAA, 14th Aerospace Sciences Meeting, January 1976, Paper Number 76-67.

10. R.A. Mugele & H.D. Evans, "Droplet Size Distribution in Sprays," Ind. & Eng. Chem., June 1951, pp. 1317-1323.

11. R.D. Gumprecht & C.M. Sliepcevich, "Scattering of Light by Large Spherical Particles," J. Phys. Chem., 57, 1953, pp. 90-95.

12. R.A. Powell & B.T. Zinn, "In Situ Measurement of the Complex Reflactive Index of Combustion Generated Particulates," Combustion Diagnostics by Nonintrusive Methods, Edited by T.D. McCay and J.A. Roux, AIAA Vol. 92, pp. 334-351.

13. Naval Postgraduate School Report No. NPS67-82-13, An Investigation of the Effectiveness of Smoke Suppressant Fuel Additives for Turbojet Applications, by J.R. Bramer, D.W. Netzer, September 1982.

INITIAL DISTRIBUTION LIST

		NO. OF COPIES
1.	Library Code, 0142 Naval Postgraduate School Monterey, CA 93943	2
2.	Department of Aeronautics Code 67 Naval Postgraduate School Monterey, CA 93943	
	Chairman	1
	D.W. Netzer	10
3.	Research Administration Code 012 Naval Postgraduate School Monterey, CA 93943	1
4.	Defense Technical Information Center Cameron Station Alexandria, VA 22314	2
5.	Chief of Naval Operations Navy Department Washington, DC 20360 (Attn: Code OP451, IP453)	2
6.	Chief of Naval Material Navy Department Washington, DC 20360 (Attn: Codes: 08T241, 044P1)	2
7.	Commander Naval Air Systems Command Washington, DC 20360 (Codes: AIR-01B, 330D, 3407, 4147A, 50184, 5341B, 53645, 536B1)	8
8.	Commanding Officer Naval Air Rework Facility Naval Air Station North Island San Diego, CA 92135	1
9.	Commander Naval Facilities Engineering Command 200 Stoval Street Alexandria, VA 22332 (Codes: 104, 032B)	2

10. Naval Construction Battalion Center — 1
Port Hueneme, CA 93043
(Codes: 25, 251, 252)

11. U.S. Naval Academy — 1
Annapolis, MD 21402
(Attn: Prof. T. Williams)

12. Arnold Engineering Development Center — 1
Arnold AFS, TN 37342
(Code: DYR)

13. Air Force Aero Propulsion Laboratory — 1
Wright-Patterson AFB, OH 45433
(Code: SFF)

14. Detachment 1 — 2
(Civil & Environmental Engineering
Division Office)
HQ ADTC (AFSC)
Tyndall AFB, FL 32401
(Code: EV, EVA)

15. Army Aviation Systems Command — 1
P.O. Box 209
St. Louis, MO 63166
(Code: EOP)

16. Eustis Directorate — 1
USA AMR & DL
Ft. Eustic, VA 23604
(Code: SAVDL-EU-TAP)

17. National Aeronautics and Space Admin. — 1
Lewis Research Center
2100 Brookpark Road
Cleveland, OH 44135
(Attn: Mail Stop 60-6 (R. Rudley))

18. Federal Aviation Administration — 1
National Aviation Facility Experimental Ctr.
Atlantic City, NJ 08405

19. Naval Air Propulsion Center — 3
Trenton, NJ 08628-0176
(Code: PE 71:AFK)

20. Naval Ocean Support Center — 2
271 Catalina Boulevard
San Diego, CA 92152
(Attn: M. Lepor, M. Harris, Code 5121)

21. Naval Air Rework Facility
Alameda, CA 94501
(Attn: G. Evans, Code 642)

END

5-87

DTIC